A&A 430, 411–419 (2005)
DOI: 10.1051/0004-6361:20034571

Astronomy & Astrophysics

The structure of elliptical galaxies in the Virgo cluster. Results from the INT Wide Field Survey⋆

G. Gavazzi[1], A. Donati[1], O. Cucciati[1], S. Sabatini[2], A. Boselli[3], J. Davies[2], and S. Zibetti[4]

[1] Universitá degli Studi di Milano-Bicocca, P.zza della Scienza 3, 20126 Milano, Italy
e-mail: [Giuseppe.Gavazzi;alessandro.donati]@mib.infn.it
[2] Department of Physics and Astronomy, Cardiff University, UK
e-mail: sabina.sabatini@astro.cf.ac.uk
[3] Laboratoire d'Astrophysique de Marseille, BP8, Traverse du Siphon, 13376 Marseille, France
e-mail: alessandro.boselli@oamp.fr
[4] Max-Planck-Institut für Astrophysik, Garching, Germany
e-mail: zibetti@mpa-garching.mpg.de

Received 24 October 2003 / Accepted 16 September 2004

Abstract. We report on a complete CCD imaging survey of 226 elliptical galaxies in the North-East quadrant of the Virgo cluster, representative of the properties of giant and dwarf elliptical galaxies in this cluster. We fit their radial light profiles with the Sersic $r^{1/n}$ model of light distribution. We confirm the result of Graham & Guzman (2003, AJ, 125, 2936) that the apparent dichotomy between E and dE galaxies in the luminosity–$\langle\mu\rangle_e$ plane no longer appears when other structural parameters are considered and can be entirely attributed to the onset of "core" galaxies at $B_T \sim -20.5$ mag. When "core" galaxies are not considered, E and dE form a unique family with n linearly increasing with the luminosity.
For 90 galaxies we analyze the $B-I$ color indices, both in the nuclear and in the outer regions. Both indices are bluer toward fainter luminosities. We find also that the outer color gradients do not show any significant correlation with the luminosity. The scatter in all color indicators increases significantly toward lower luminosities, e.g. galaxies fainter than $B_T \sim -15$ have a $B-I$ spread > 0.5 mag.

Key words. galaxies: elliptical and lenticular, cD – galaxies: fundamental parameters – galaxies: clusters: individual: Virgo

1. Introduction

The widespread belief that dwarf (dE) and giant (E) elliptical galaxies form two distinct families brought unanimous consent that separate mechanisms are responsible for their formation and evolution (see Ferguson & Binggeli 1994, for a review). Alleged evidence for a structural dE/E dichotomy includes: i) the light profiles of dEs follow exponential laws (Binggeli et al. 1984), as opposed to their giant counterparts that follow the $r^{1/4}$ law (de Vaucouleurs 1948); ii) scaling relations of the structural parameters r_e, the effective radius, and $\langle\mu\rangle_e$, the mean surface brightness within r_e, with the total luminosity indicate that dEs of increasing luminosity have greater surface brightness while giant Es show the reverse trend (Binggeli & Cameron 1991; Binggeli et al. 1984). Moreover they occupy distinct loci in the r_e vs. $\langle\mu\rangle_e$ plane: giants have dimmer surface brightness with increasing radius (Kormendy & Djorgowski 1989), while dEs do not.

Hydrodynamical simulations, including mass loss from stars and gas heating and cooling, show that gravitational instability of primeval density fluctuations (with or without dark matter) results in the formation of elliptical galaxies with brighter $\langle\mu\rangle_e$ at high luminosity, as observed in the dE regime, without showing any dichotomy, i.e. the bright objects result as scaled-up versions of the less luminous systems (Athanassoula 1993).

Various mechanisms involving merging have been proposed for the formation of E galaxies that are consistent with the alleged dE/E dichotomy. Dwarf Es in clusters might derive from the harassment of dwarf spiral galaxies (Moore et al. 1996, 1998; Mao & Mo 1998; Mayer et al. 2001), while giant E galaxies might arise from the merger of two spiral galaxies or from the multiple merging of dEs (Kauffmann et al. 1993).

There is however some observational evidence arguing for a continuity rather than a dichotomy between dEs and Es: i) the $U-V$ (Caldwell 1983) and $B-H$ (Scodeggio et al. 2002) colors and the metallicity are found to smoothly increase with luminosity; ii) the Near-IR light concentration index (Scodeggio et al. 2002) and the central surface brightness (Caldwell & Bothun 1987; Jerjen & Binggeli 1997) increase monotonously with the absolute magnitude; iii) no clear

⋆ Table 2, Figs. 13 and 14 are only available in electronic form at http://www.edpsciences.org

dichotomy can be assessed between giants and dwarfs in the Near-IR $\langle\mu\rangle_e - R_e$ and fundamental plane relations (Zibetti et al. 2002). Whether there is kinematic evidence for the dE/E dichotomy remains a controversial issue: the preliminary conclusion of Geha et al. (2001) that dE and E are both not rotation-supported systems has been subsequently questioned by the same authors (Geha et al. 2003) who concluded, in agreement with Pedraz et al. (2002) and van Zee et al. (2004), that dE galaxies can have significant rotation.

Moreover the very existence of the aforementioned dE/E dichotomy has been recently questioned by Graham & Guzman (2003; GG03 hereafter). These authors argued that the dichotomy is apparent, as it derives from the use of exponential and de Vaucouleurs laws to decompose the light profiles of dE and E galaxies respectively, combined with the use of $\langle\mu\rangle_e$ as representative of the surface brightness. When μ_0 is analyzed, as obtained from the inner extrapolation of Sersic $r^{1/n}$ laws (Sersic 1968), no dichotomy remains.

Stimulated by the conclusions of GG03 we undertook this project aimed at re-assessing the relations involving the size, the surface brightness and the luminosity of dE-E galaxies, all ingredients entering in the determination of the fundamental plane. The present analysis is carried out using a sample which by selection should be representative of the properties of dE-E galaxies in one cluster.

The Virgo cluster, owing to its relatively small distance from us (17 Mpc), represents an appropriate testbed for such a study, although its significant line-of-sight depth (Gavazzi et al. 1999; Solanes et al. 2002) and sub-clustering makes it not ideal. In spite of their low surface brightness, dwarf galaxies as faint as 19 mag are within reach of mid-size telescopes and seeing limitations are less severe when studying galaxies at the distance of Virgo than objects 5 times further away such as the Coma galaxies that require the superior resolution of HST. Since their luminosity function was determined (e.g. Sandage et al. 1985), early systematic studies of dwarf galaxies in Virgo were based on photographic material (Binggeli & Cameron 1991, 1993; Young & Currie 1998). Modern photometry obtained with panoramic detectors exists today for many Virgo galaxies (e.g. Caon et al. 1993; Gavazzi et al. 2003; Barazza et al. 2003) and many have been observed with the HST (e.g. Faber et al. 1997; Cote et al. 2004). A large stretch of the Virgo cluster was mosaiced with the Isaac Newton Telescope in what is known as the "Virgo Wide Field Survey" (Sabatini et al. 2003). These data are used in the present analysis to re-assess the issue of the dE/E dichotomy.

The analyzed sample is described in some detail in Sect. 2. Sections 3 and 4 describe the method used to derive the light profiles and their fitting with Sersic models. The $B - I$ color analysis and the analysis of the various structural B-band parameters are carried out in Sect. 5 and the conclusions of our work are briefly summarized in Sect. 6.

2. The sample

The present structural analysis of elliptical galaxies is focused on the North-East quadrant of the Virgo cluster delimited by $\alpha > 12^h20^m00^s$ and $\delta > 10°00'00''$ (see Fig. 1). With this choice we try to include in the analysis genuine members of cluster A (M 87) and to exclude members of other dynamical units within the Virgo cluster, namely cluster B (M 49), clouds M and W which are located to the West and South of the above region, showing significant 3-D structure, i.e. distances in excess of 6 (cluster B) and 15 Mpc (M, W clouds) with respect to cluster A that we assume at 17 Mpc distance (Gavazzi et al. 1999).

Our structural analysis requires the availability of imaging material (CCD images) suitable for deriving the light profiles according to the method described in Sect. 4. The imaging data are taken from the Wide Field Survey (WFS), horizontal (WFH) and vertical (WFV) strips delimited by the solid rectangles in Fig. 1. B-band data are available for both strips. Moreover in the vertical strip we had access to I-band data to study the $B - I$ color of galaxies in this region (see Sect. 5.2). WFS images are in principle available for all (439) $m_p \leq 20$ galaxies in the Virgo Cluster Catalog (VCC; Binggeli et al. 1985) projected onto the WFS region[1]. We restricted however the present analysis to the 251 galaxies with $m_p \leq 19$, with morphological type dE or E, that are spectroscopically confirmed members ($V < 3000$ km s^{-1}) or possible members according to Binggeli et al. (1985, 1993). We were able to fit meaningful B Sersic profiles to 226 galaxies out of 251 because 18 were not observed and the remaining 7 were too faint or the images were of insufficient quality. Summarizing, B-band structural information is available for 226/251 objects, thus with a completeness of 90%. The I-band structural information is available for 90 objects. The sample completeness is detailed in Table 1. At the assumed distance of 17 Mpc ($\mu = -31.15$), the limit of $m_p = 19$ mag corresponds to $M_p = -12.15$. Therefore the analyzed sample can be considered representative of the properties of dE-E galaxies in the N-W portion of the Virgo cluster. Figure 2 illustrates the luminosity function of dE-E galaxies included in the present analysis. It is in full agreement with the one derived by Sandage et al. (1985, see their Fig. 11) for the entire VCC, once re-normalized to account for the 28% coverage of the WFS with respect to the entire cluster and for the different distance modulus assumed.

3. The imaging data

The Virgo Wide Field Survey was carried out with the Wide Field Camera (WFC) at the Isaac Newton Telescope (INT) (Sabatini et al. 2003).

The horizontal strip was covered with 55 overlapping fields of 34 × 22 arcmin each, using 3 of the 4 chips of 4000 × 2000 pixel (each of 0.333 arcsec on the sky)

[1] Nine VCC galaxies in the WFH (VCC 1143, 1147, 1216, 1335, 1336, 1482, 1486, 1795, 1886) and nine in the WFV (281, 333, 400, 437, 723, 742, 769, 863, 884) were not observed in the B-band because they lie in the gaps between adjacent chips of the WFC; similarly 15 objects in the WFV (I-band) (VCC 400, 413, 505, 578, 663, 666, 677, 723, 751, 769, 797. 798. 857, 882, 884).

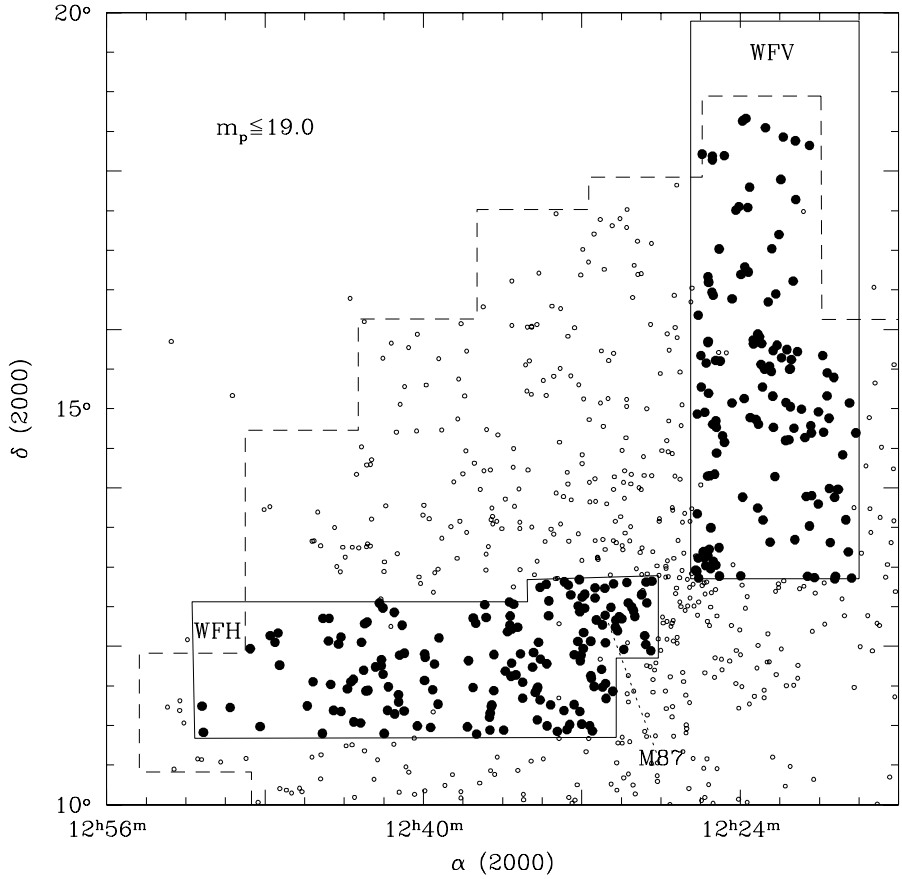

Fig. 1. The N-E region of the Virgo cluster including galaxies with $m_p \leq 19.0$. The dashed line represents the boundary of the VCC catalog. The rectangles include the studied WFH and WFV areas, covering approximately 26 deg^2. The location of M 87 is indicated.

constituting the WFC[2]. For this strip we had access only to the *B*-band (Johnson) data. The observations were carried out in nearly photometric conditions with a seeing varying from 1 to 3 arcsec, with a mean of 1.6 arcsec (see Fig. 3). An integration time of 750 s was used.

The Vertical strip was covered in both the *B*- and the *I*-band. The *B*-band survey was carried out with 80 overlapping fields, using 3 of the 4 chips of the WFC, each exposed for 750 s. The observations were taken in nearly photometric conditions with a seeing varying from 1.2 to 3.5 arcsec, with a mean of 2.1 arcsec.

The *I*-band survey consists of 73 overlapping fields[3], each exposed for 1000 s. The observations were carried out in nearly photometric conditions with a seeing varying from 1 to 2.5 arcsec, with a mean of 1.3 arcsec.

4. Data reduction

The reduction of the *B*-band science frames was performed as described in Sabatini et al. (2003). The zero point of all images was obtained from the "CASU INT Wide Field Survey Home Page" (`http://www.ast.cam.ac.uk/~wfcsur/index.php`).

The *I*-band images suffer from fringing, producing unwanted structures in the background. However for this band we could access images produced by all 4 chips of the WFC, including the top, redundant, vignetted chip. Several galaxies were observed in non-vignetted parts of this chip as well as in other chips of other frames. In these cases we combined two independent sets of measurements to reduce the fringing.

Because of the significantly better seeing in the *I*- compared to the *B*-band, the *I*-band profile decomposition (see next section) was performed twice: once on the original data,

Table 1. The sample. For each band the number of dE-E galaxies in the WFS (separately for the Horizontal and Vertical strips) with $m_p \leq 19$ mag. that are members or possible members, to which we have been able to fit a Sersic profile is given. The denominator gives the number of galaxies in the VCC at the same magnitude limit.

	B	*I*
Strip	$m_p \leq 19$	$m_p \leq 19$
WFH	131/149 (88%)	–
WFV	95/102 (93%)	90/102 (89%)

[2] The WFC is made of 3 chips, one on top of the other, and of one orthogonal chip on one side. The top horizontal chip is partly vignetted. This chip was not used in the *B*-band survey, but it was considered in the *I*-band (see next section).

[3] The 7 missing *I*-band frames lie at $\delta > 18°00'$, in a region almost devoid of VCC galaxies.

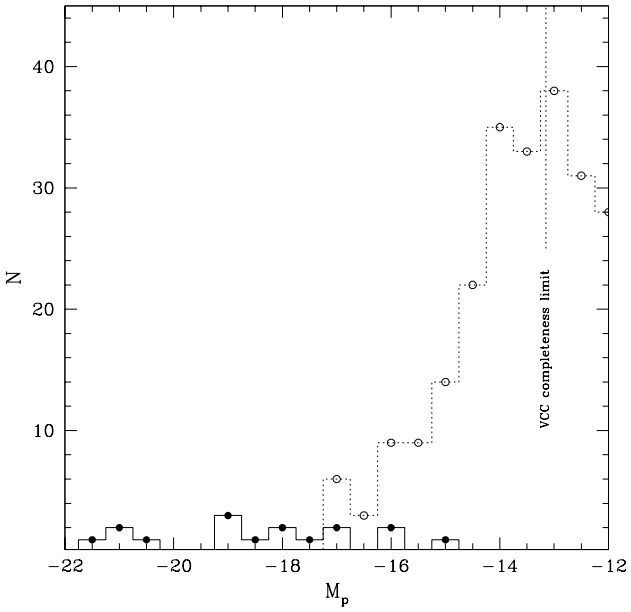

Fig. 2. The luminosity function of E (filled symbols) and dE (open symbols) in the WFS. The completeness limit of the VCC (m_p = 18) is indicated.

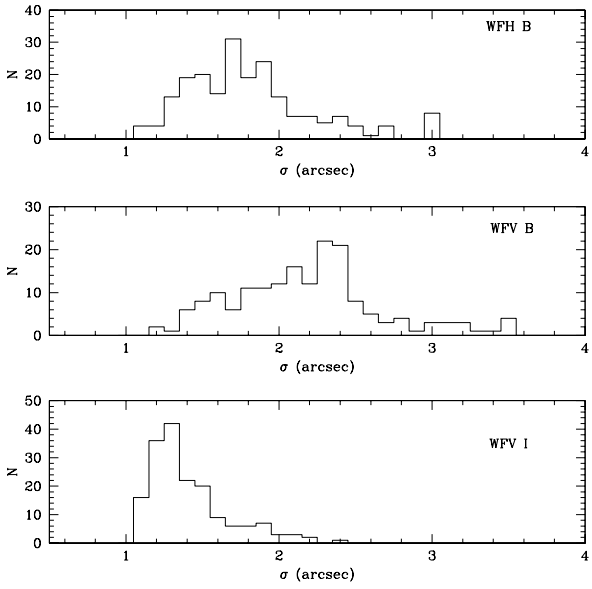

Fig. 3. Distribution of the seeing in the WFS.

once on degraded images obtained convolving the images to the *B*-band seeing.

4.1. Profile decomposition

The profile decomposition is performed using the method described in Gavazzi et al. (2000, 2001) which is based on the IRAF environment and relies on the STSDAS[4] package and on GALPHOT (developed for IRAF- STSDAS mainly by W. Freudling, J. Salzer, and M.P. Haynes and adapted by M. Scodeggio, P. Franzetti and S. Zibetti).

For each frame the sky background is determined as the mean number of counts measured in regions of "empty" sky, and it is subtracted from the frame.

The 2-dimensional light distribution of each galaxy is fitted with elliptical isophotes, using a procedure based on the task *ellipse*, (STSDAS *ISOPHOTE* package; Jedrzejewski 1987; Busko 1996), which allows the interactive masking of unwanted superposed stars and galaxies. Starting from an interactively centered ellipse, the fit maintains as free parameters the ellipse center, ellipticity and position angle. The ellipse semi-major axis is incremented by a fixed fraction of its value at each step of the fitting procedure. The routine halts when the surface brightness found in a given annulus equals the the average sky value, and then restarts decrementing the initial semi-major axis toward the center. The fit fails to converge for some very faint galaxies. In these cases we keep fixed one or more of the ellipse parameters.

The resulting surface brightness profiles are fitted using the Sersic model (Sersic 1968) of light distribution:

$$I(r) = I_0 \mathrm{e}^{-(r/r_0)^{1/n}} \quad (1)$$

where I is the surface brightness (in intensity) at the radius r (along the major axis), I_0 is the central surface brightness, r_0 the scale length and n is the dimensionless shape parameter that determines the curvature of the profile. This model is a simple generalization of de Vaucouleurs (n = 4) and exponential (n = 1) law. The surface brightness profiles are fitted with this model in the magnitude representation:

$$\mu(r) = \mu_0 + 1.086(r/r_0)^{1/n} \quad (2)$$

where $\mu(r)$ is the surface brightness (in magnitude) at the radius r (along the major axis), μ_0 is the central surface brightness.

The fit is performed using a weighted least squares method from a radius equal to one seeing disk (σ)(with the exceptions discussed in Sect. 4.2), out to the outermost significant isophotes, i.e. when the surface brightness equals the average sky value. We deliberately avoid fitting the nuclear features.

The total asymptotic magnitude $B_T = -2.5\log(F_T)$ is obtained by adding to the flux measured ($F_{\rm last}$) within the outermost significant isophote ($r_{\rm last}$) the extra flux extrapolated to infinity along the model:

$$F_{\rm extra} = 2\pi I_0(1-\epsilon)nr_0^2 \left[\Gamma(2n) - \gamma\Big(2n, \Big(\frac{r_{\rm last}}{r_0}\Big)^{1/n}\Big)\right] \quad (3)$$

where ϵ is the ellipse eccentricity, Γ and γ are the complete and incomplete Gamma functions respectively. The effective radius r_e (the radius containing half of the total light) and the effective surface brightness $\langle\mu\rangle_e$ (the mean surface brightness within r_e), r_{25}, r_{75} (the radii that enclose 25% and 75% of the total light) of each galaxy are computed empirically

[4] IRAF is the Image Analysis and Reduction Facility made available to the astronomical community by the National Optical Astronomy Observatories, which are operated by AURA, Inc., under contract with the US National Science Foundation. STSDAS is distributed by the Space Telescope Science Institute, which is operated by the Association of Universities for Research in Astronomy (AURA), Inc., under NASA contract NAS 5–26555.

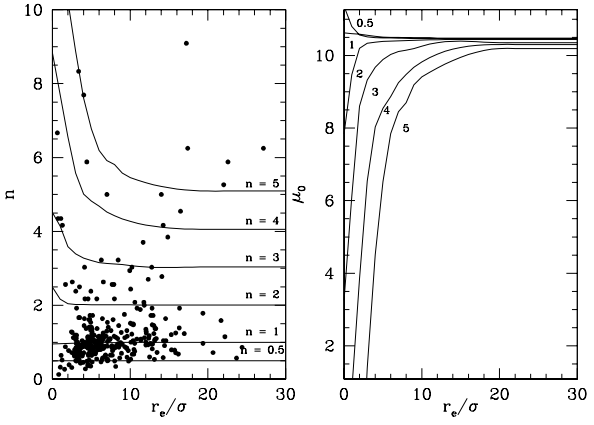

Fig. 4. The effect of the seeing on n (*left*) and on μ_0 (*right*) as derived from the simulations (lines) for various n. Dots give the distribution of the observed points in the $n - r_e/\sigma$ plane.

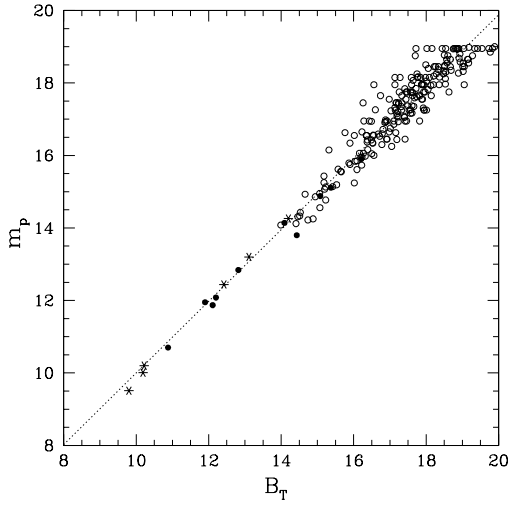

Fig. 5. Comparison of B_T from this work with m_p from the VCC. The dotted line gives the bisector linear regression. In this and in the following figures (unless otherwise specified) empty symbols refer to dEs, filled symbols to Es and asterisks to "core" galaxies.

from B_T, i.e. are derived from the data, using the Sersic models to extrapolate from the last measured magnitude to infinity. Similarly we compute the concentration index (C_{31}), defined in de Vaucouleurs (1977) as the ratio between r_{75} and r_{25}. Fits to the B-band light profiles were obtained for 136 galaxies, as given in Fig. 13, and to $B + I$-band light profiles for 90 objects, as given in Fig. 14.

4.2. The effects of the seeing

Attempts to model the effects of the seeing on Sersic parameters can be found in the literature, e.g. by Trujillo et al. (2001a,b) who modeled the effect of Gaussian and Moffat convolution on Sersic profiles. To illustrate this issue we used some simple simulations. We constructed sets of artificial images injecting fake Sersic galaxies with zero ellipticity, constant μ_0, fixed $r_e = 10$ arcsec and Sersic index n varying from 0.5 to 5 on a sky background with noise characteristics similar to the INT frames. To simulate the effects of the seeing the images were convolved with Gaussians of $FWHM$ (σ) ranging from 0.5 to 10 arcsec, so that r_e/σ varies between 20 and 1, mimicking the range covered by the real data. We fitted circular isophotes and measured the Sersic parameters on the blurred images with the same tools and criteria used for real data (i.e. disregarding the data points within the seeing disk). Figure 4 illustrates how the measured Sersic parameters n and μ_0 vary as a function of r_e/σ (lines). Dots give the observed distribution in the $n - r_e/\sigma$ plane. From Fig. 4 it is apparent that increasing corrections to the Sersic parameters are required with increasing n and decreasing r_e/σ. For $n \geq 3$ the seeing produces overestimates of n (thus enhancing the central surface brightness μ_0) because flux from the central cusp is distributed in the surrounding pixels producing a steepening of the inner profile.

As a result of the simulations we decided not to try to correct the individual Sersic parameters (that are not independent of one another), but to modify our fitting strategy in the case of $n \geq 3$, i.e. excluding from the fit the data points within 2× the seeing disk σ.

5. Results

The B-band parameters derived in this work are listed in Table 2. Magnitudes and surface brightness are corrected for extinction in our Galaxy according to Burstein & Heiles (1982) (due to the high galactic latitude of the Virgo cluster this results in a small 0.05 mag correction on average included in Cols. 4, 6, 7, and 9).

5.1. Consistency test

The quality of the measurements in Table 2 is first checked by comparing the total asymptotic magnitudes (B_T) derived in this work with m_p given in the VCC (see Fig. 5). B_T is found in linear proportionality with m_p. The bisector linear regression (see Feigelson & Babu 1992) is:

$$m_p = +0.11 + 0.99 B_T (R = 0.96)$$

where R is the Pearson regression coefficient.

Figure 6 illustrates the comparison between the parameters derived in this work on CCD frames with the parameters derived on photographic material by Young & Currie (1998, VPC) for the 42 common galaxies (left) and by Binggeli & Jerjen (1998) (based on photographic data of Binggeli & Cameron 1991) for the 37 common galaxies (right). The agreement between the two sets of measurements is satisfactory, except for some deviating objects marked individually in the figure with their VCC denominations. The three most discrepant objects (i.e. VCC 748, 833, 1565) have B_T derived in this work consistent within 0.28 mag with m_p from the VCC, differing by more than 1.5 mag from the VPC values. Furthermore we checked the n index on the profiles of VCC 748, 1148 and 1308 and confirmed that the value found in this work is correct.

We remark that 18 galaxies are in common between this work, Young & Currie (1998) and Binggeli & Jerjen (1998). For these objects we compare the Sersic parameters on 3 independent data-sets and we conclude that the consistency is best

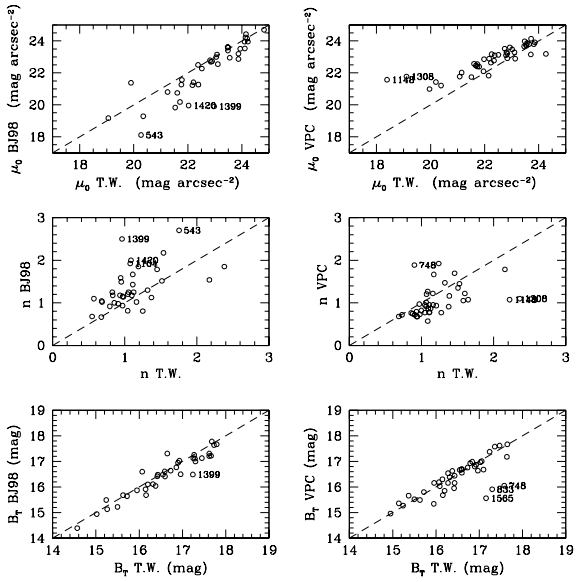

Fig. 6. Comparison among structural parameters derived in this work and by Young & Currie (1998) for 42 common galaxies (*right*) and by Binggeli & Jerijn (1998) for 37 common galaxies (*left*).

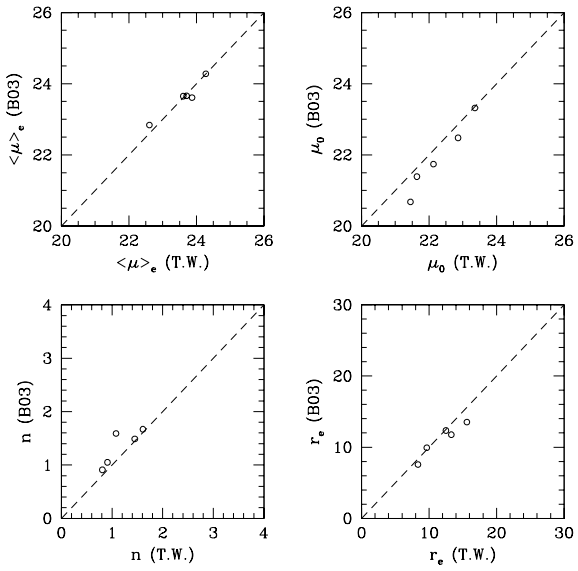

Fig. 7. Comparison among structural parameters derived in this work and by Barazza et al. (2003) for 5 common galaxies.

between this work and the VPC and worst between Young & Currie and Binggeli & Jerjen (1998). In other words the average errors in the VPC are approx. 1.5 times larger than those in this work while those of Binggeli & Jerjen (1998) are approx. 3 times larger than those in this work.

Indeed when we compare the results of this work with those obtained by Barazza et al. (2003) on CCD material for the 5 common galaxies (see Fig. 7) we find a high consistency.

5.2. B−I color analysis

Using 90 galaxies in the WFV that have been observed both in the *B* and in the *I*-band we analyze in this section the $B-I$ color properties of dE-E galaxies. For these objects the *B* band Sersic

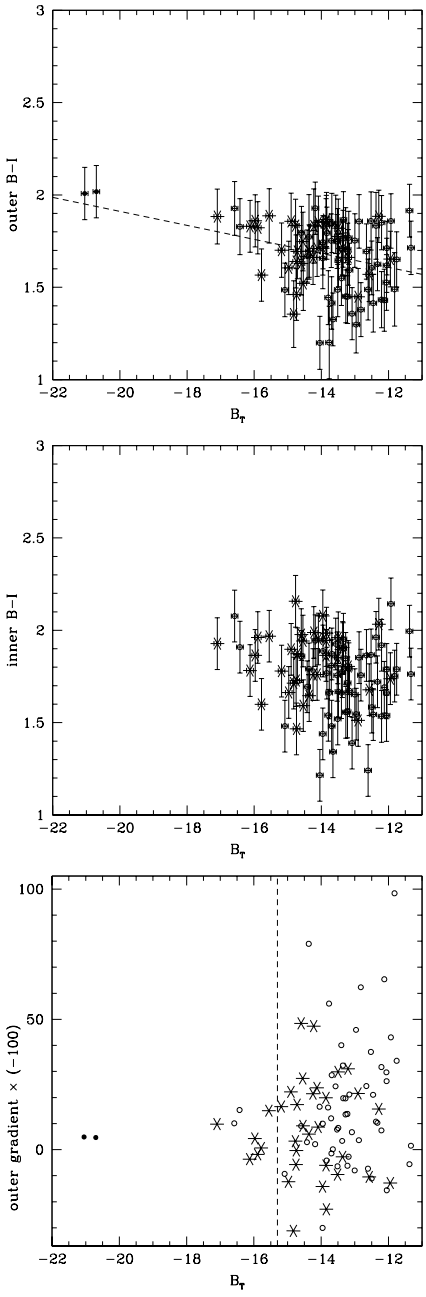

Fig. 8. The outer $B-I$ color index (*top*); the inner $B-I$ color index (*middle*; the two brightest objects are missing in this panel because they are both saturated) and the outer $B-I$ gradient (*bottom*) as a function of B_T. In this figure filled dots represent giant Es, empty dots dEs, asterisks Nucleated dEs.

parameters were compared with two sets of similar *I* band parameters, i.e. those derived from the original *I* images and from the *I* images convolved to the *B*-band seeing. The agreement between the *B* and *I* parameters is satisfactory and it improves when the *B* parameters are compared with those obtained from the blurred *I* images.

For these objects we also compute the outer $B-I$ color index in the radial interval between $r > 1.5 \times \sigma$ and (two points before) the last significant measurement, as representative of the galaxy color outside the nucleus, avoiding the least reliable, outermost points. Figure 8 (top) gives the color–magnitude

diagram obtained in this way, showing the expected trend of blueing toward fainter luminosities (see Baldry et al. 2004). We remark however that our WFV data-set contains too few giant E galaxies to explore the relation at high luminosity. It appears that, fainter than $B_T = -16$, the scatter in the relation becames increasingly large.

For the same set of galaxies we also compute the "outer color gradient" as the slope of the line fitted to the $B - I$ color profile in the radial interval between $r > 1.5 \times \sigma$ and (two points before) the last significant measurement. When plotting the outer gradient we follow the convention of Vader et al. (1988) of "positive" gradients when the the center is redder. Figure 8 (bottom) shows the outer gradients as a function of the B luminosity, revealing no significant correlation. We do not confirm the trend found by Vader et al. (1988) in a brighter ($B_T < -15.3$, vertical line) sample who claimed that brighter galaxies have more positive gradients (outer envelopes bluer than inner regions) than fainter objects. Our fainter sample shows that this trend does not hold at faint luminosities where the outer gradients show a tremendous scatter.

Figure 8 (middle) shows the inner (or nuclear) color index obtained as the difference of the B and I magnitudes integrated within $1 \times \sigma$. There is only a weak tendency for redder nuclei in brighter objects, but again with a large uncertainty.

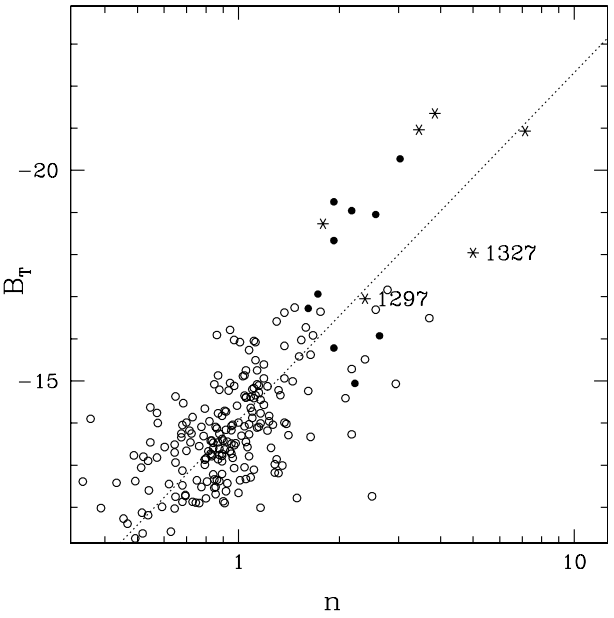

Fig. 9. The dependence of n from B_T. The dashed line gives the bisector linear regression.

5.3. Correlations among B-band structural parameters

Guided by the work of GG03 who based their study on a sample of 18 dEs in Coma observed with the HST, combined with 232 elliptical galaxies taken from the literature, we analyze in this Section several correlations among structural parameters of dE-E galaxies in the Virgo cluster that are derived using the Sersic model.

We remark that the sample of Virgo elliptical galaxies we are using is 90% complete at $m_p < 19$. In other words the density of points in the various plots reflects the real frequency in the parameter space of Virgo galaxies.

We begin by remarking, in full agreement with GG03 and Caon et al. (1993), that in our sample there is a significant linear increase of the Sersic index n with the system luminosity (see Fig. 9). Using the bisector linear regression we find:

$$\log(n) = -0.12 \times B_T + 1.71 \ (R = -0.72). \quad (4)$$

All dEs with $B_T > -17$ have Sersic index $n \lesssim 2$ while the few giant Es have n as high as 7.

Secondly we show in Fig. 10 (top) that the relation B_T versus $\langle\mu\rangle_e$, extensively studied by Binggeli & Cameron (1991), Binggeli et al. (1984) and Ferguson & Binggeli (1994) shows the existence of two separate regimes: dwarf elliptical galaxies having brighter surface brightness with increasing luminosity, and giants showing the reverse trend. Furthermore the relation between the effective surface brightness and the radius (see Fig. 10, middle) is of inverse proportionality for giant ellipticals (Kormendy & Djorgowski 1989), i.e. smaller radii at brighter mean surface brightness, while dEs show a sparse relation (see also Capaccioli & Caon 1991). Third we show (bottom) that the scale $\log R_e$ increases with B_T more rapidly for giant Es than for dEs (see Binggeli et al. 1984).

In all panels of Fig.10 it appears that some dichotomy occurs in passing from dEs to Es. However, as stressed for the first time by GG03, all bright galaxies showing deviant trends in this figure are the "partially evacuated core" or "core" galaxies that show a flat slope in the inner $\lesssim$100 pc ($\lesssim$1.2 arcsec at the distance of Virgo), as opposed to the "normal" galaxies with a central cusp (that Faber et al. 1997, define as "power-law" galaxies). It should be noted that the region of the Virgo cluster mapped with completeness in this work does not contain many "core" galaxies, beside M 84, M 86 and M 87 (the brightest objects in Fig. 10). Most "core" objects found in other clusters by Faber et al. (1997) are much more luminous ($-21 < B_T < -24$) cD galaxies with large outer envelopes that are absent in Virgo. These galaxies obey Sersic laws only in the outer profiles and Graham et al. (2003b) have developed a formalism to model their profiles in their full extent. The rectangles in Fig. 10 represent the loci occupied by them. Notice that the M 32-like objects (e.g. VCC 1297 and 1327) (both core galaxies) represent the low-luminosity continuation of the core regime.

The E-dE dichotomy no longer appears when B_T is plotted as a function of μ_0 in Fig. 11. GG03 conclude that "normal" dE-E galaxies have increasingly brighter central surface brightness with increasing luminosity, until the onset of "core" formation in elliptical galaxies at $B_T \sim -20.5$ mag. Together with GG03 we conclude that among "normal" E-dE galaxies there is no dichotomy in the structural parameters. Only the "core" galaxies seem structurally different, perhaps due to a different formation mechanism (see the discussion in Graham et al. 2003b).

Given the significant correlation between B_T and log n, which clearly indicates a smooth, continuous transition from

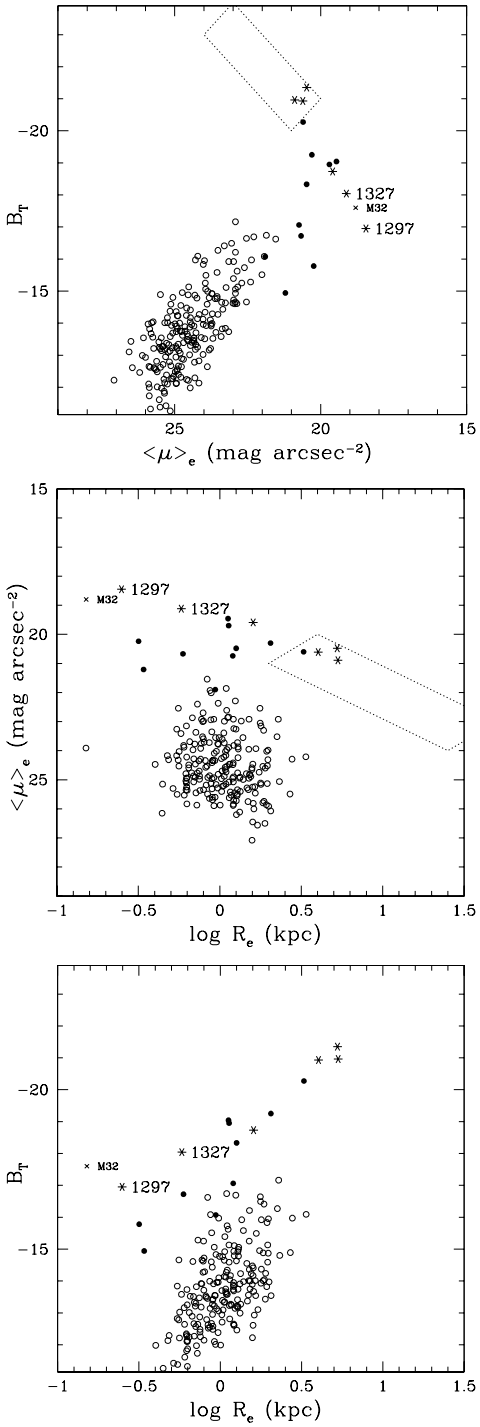

Fig. 10. Correlations among structural parameters of dE-E galaxies in the Virgo cluster. B_T vs. $\langle\mu\rangle_e$ (*top*); $\langle\mu\rangle_e$ vs. log R_e (*middle*); B_T vs. log R_e (*bottom*). The position of M 32 (scaled to the distance of Virgo and corrected for $B-V=1$) as given by Faber et al. (1997) is marked with a cross. The dotted rectangle represents the loci of luminous "core" galaxies adapted from GG03.

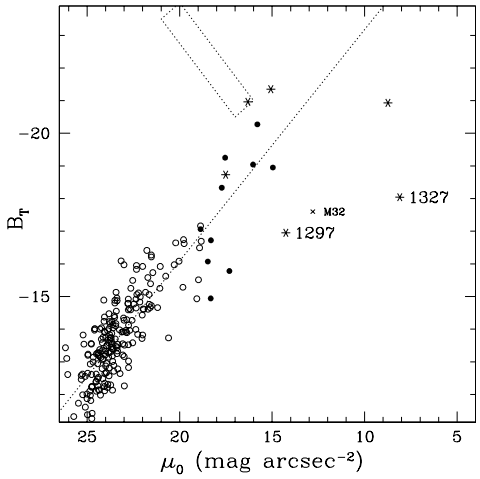

Fig. 11. Correlation between B_T and μ_0 for dE-E galaxies in the Virgo cluster. The position of M 32 is marked with a cross. The dotted rectangle represents the loci of luminous "core" galaxies adapted from GG03. The dashed line gives the bisector linear regression.

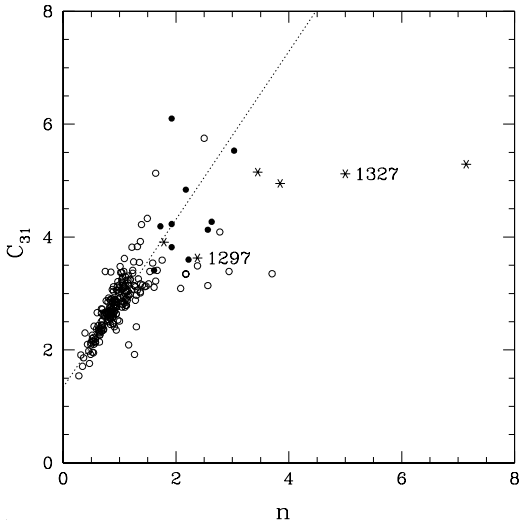

Fig. 12. Distribution of C_{31} versus n. The dashed line gives the bisector linear regression: $C_{31}=1.49\times n+1.33$.

the dE to the E regime, and the (analytically[5] expected) correlation between the light concentration index C_{31} and the Sersic index n (see Fig. 12), it is not surprising that C_{31} increases linearly with the total luminosity B_T. This has been known since our Near-IR survey, as stressed by Scodeggio et al. (2002).

An additional element of continuity between dE and E is the color–luminosity diagram of Fig. 8 The gradual increase of the $B-I$ index with increasing luminosity, resulting from the metallicity–mass relation (Arimoto & Yoshii 1987), encompasses the whole dE-E sequence, although with a larger scatter among dEs.

6. Summary and conclusions

We carried out a CCD survey of the North-East quadrant of the Virgo cluster containing ∼30% of the galaxies in this cluster. We analyzed images for 226 and 90 galaxies respectively in the B- and I-band, representative of the properties of giant and dwarf elliptical galaxies in this cluster.

[5] C_{31} and n are expected to have a perfect correlation in the Sersic model. However in our definition C_{31} is empirically determined from the data.

We fit the galaxies' radial light profiles with the Sersic $r^{1/n}$ model of light distribution obtaining the structural parameters n, $\langle\mu\rangle_e$, r_e, B_T, C_{31} and μ_0. We find that the Sersic model provides an adequate representation of the observed light profiles of dE and E galaxies spanning 9 mag.

We confirm the result of Graham & Guzman (2003) that the apparent dichotomy between E and dE galaxies in the luminosity–$\langle\mu\rangle_e$ plane is due to the onset of "core" formation in elliptical galaxies at $B_T \sim -20.5$ mag. The segregation among dE and E no longer appears when other structural parameters are considered.

For 90 galaxies in the WFV we analyze the $B-I$ color indices, both in the nuclear and in the outer regions. Both indices are bluer toward fainter luminosities, however the scatter in these relations increases significantly toward lower luminosities. Moreover we find that the outer color gradients do not show any significant correlation with the luminosity.

Acknowledgements. We wish to thank Luca Cortese for the useful discussions. This work could not have been completed without the NASA/IPAC Extragalactic Database (NED) which is operated by the Jet Propulsion Laboratory, Caltech under contract with NASA. This research has made use also of the GOLDMine Database (`http://goldmine.mib.infn.it`).

References

Arimoto, N., & Yoshii, Y. 1987, A&A, 173, 23
Athanassoula, E. 1993, Proc. ESO/OHP Conf. on Dwarf Galaxies
Baldry, I. K., Glazebrook, K., Brinkmann, J., et al. 2004, ApJ, 600, 681
Barazza, F. D., Binggeli, B., & Jerjen, H. 2003, A&A, 407, 121 (B03)
Binggeli, B., Sandage, A., & Tammann, G. 1985, AJ, 90, 1681 (VCC)
Binggeli, B., & Cameron, L. M. 1991, A&A, 252, 27
Binggeli, B., & Cameron, L. M. 1993, A&A, 98, 297
Binggeli, B., & Jerjen, H. 1998, A&A, 333, 17 (BJ98)
Binggeli, B., Sandage, A., & Tarenghi, M. 1984, AJ, 89, 64
Binggeli, B., Popescu, C. C., & Tammann, G. A. 1993, A&AS, 98, 275
Burstein, D., & Heiles, C. 1982, AJ, 87, 1165
Busko, I. 1996, Proc. Fifth Astronomical Data Analysis Software and Systems Conf., ed. G. H. Jacoby, & J. Barnes, 101, Tucson PASP Conf. Ser., 139
Caldwell, N. 1983, AJ, 88, 804
Caldwell, N., & Bothum, G. D. 1987, AJ, 94, 1126
Caon, N., Capaccioli, M., & D'Onofrio, M. 1993, MNRAS, 265, 1013
Capaccioli, M., & Caon, N. 1991, MNRAS, 248, 523
Cote, P., Blakeslee, J. P., Ferrarese, L., et al. 2004, ApJS, 153, 223
de Vaucouleurs, G. 1948, Annales d'Astrophysique, 11, 247
de Vaucouleurs, G. 1977, in Evolution of Galaxies and Stellar Populations, ed. R. Larson, & B. Tinsley (New Haven: Yale University Observatory), 43
Faber, S. M., Tremaine, S., Ajhar, E., et al. 1997, AJ, 114, 1771 (F97)
Feigelson, E. D., & Babu, G. J. 1992, ApJ, 397, 55
Ferguson, H. C., & Binggeli, B. 1994, A&AR, 6, 67
Gavazzi, G., Boselli, A., Scodeggio, M., Belsole, E., & Pierini, D. 1999, MNRAS, 304, 595
Gavazzi, G., Franzetti, P., Scodeggio, M., Boselli, A., & Pierini, D. 2000, A&A, 361, 863
Gavazzi, G., Zibetti, S., Boselli, A., et al. 2001, A&A, 372, 29
Gavazzi, G., Boselli, A., Donati, A., Franzetti, P., & Scodeggio, M. 2003, A&A, 400, 451
Geha, M., Guhathakurta, P., & van der Marel, R. P. 2001, Am. Astr. Soc. Meeting, 199
Geha, M., Guhathakurta, P., & van der Marel, R. P. 2003, AJ, 126, 1794
Graham, A. W., & Guzman, R. 2003, AJ, 125, 2936 (GG03)
Graham, A. W., Erwin, P., Trujillo, I., & Asensio Ramos, A. 2003b, AJ, 125, 2951
Jedrzejewski, R. 1987, MNRAS, 226, 747
Jerjen, H., & Binggeli, B. 1997, in The Nature of Elliptical Galaxies, ed. M. Arnaboldi, G. S. Da Costa, & P. Saha (San Francisco: ASP), ASP Conf. Ser., 116, 239
Kauffmann, G., White, S. D. M. & Guiderdoni, B. 1993, MNRAS, 264, 201
Kormendy, J., & Djorgovski, S. 1989, ARA&A, ASP Conf. Ser., 116, 27, 235
Mao, S., & Mo, H. J. 1998, MNRAS, 296, 847
Mayer, L., Governato, F., Colpi, M., et al. 2001, ApJ, 559, 754
Moore, B., Katz, N., Lake, G., Dressler, A., & Oemler, A., Jr. 1996, Nature, 379, 613
Moore, B., Lake, G., & Katz, N. 1998, ApJ, 495, 139
Pedraz, S., Gorgas, J., Cardiel, N., Sánchez-Blázquez, P., & Guzmán, R. 2002, MNRAS, 332, L59
Sabatini, S., Davies, J., Scaramella, R., et al. 2003, MNRAS, 341, 981
Sandage, A., Binggeli, B., & Tammann, G. A. 1985, AJ, 90, 1759
Scodeggio, M., Gavazzi, G., Franzetti, P., et al. 2002, A&A, 384, 812
Sersic, J. L. 1968, Atlas de Galaxes Australes, Cordoba Obs. Astron., Univ. Nac. Corodba
Solanes, J. M., Sanchis, T., Salvador-Solé, E., Giovanelli, R., & Haynes, M. P. 2002, AJ, 124, 2440
Trujillo, I., Aguerri, J. A. L., Cepa, J., & Gutiérrez, C. M. 2001a, MNRAS, 321, 269
Trujillo, I., Aguerri, J. A. L., Cepa, J., & Gutiérrez, C. M. 2001b, MNRAS, 328, 977
Vader, J. P., Vigroux, L., Lachieze-Rey, M., & Souviron, J. 1988, A&A, 203, 217
van Zee, L., Skillman, E. D., & Haynes, M. P. 2004, AJ, 128, 121
Young, C. K., & Currie, M. J. 1998, A&AS, 127, 367 (VPC)
Zibetti, S., Gavazzi, G., Scodeggio, M., Franzetti, P., & Boselli, A. 2002, ApJ, 579, 261

Online Material

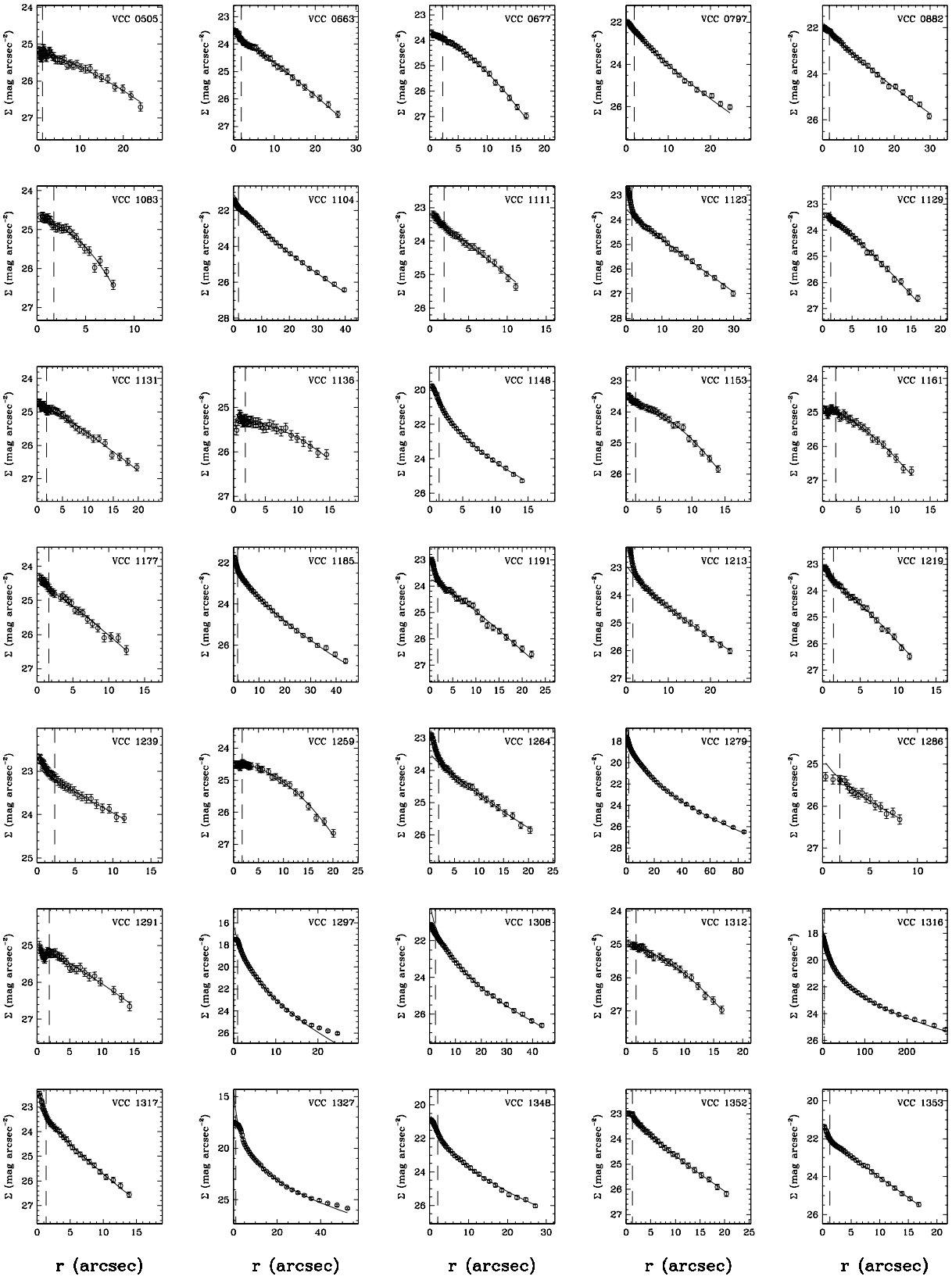

Fig. 13. The 136 individual *B*-band profiles and their Sersic fit. The vertical dashed line marks the seeing.

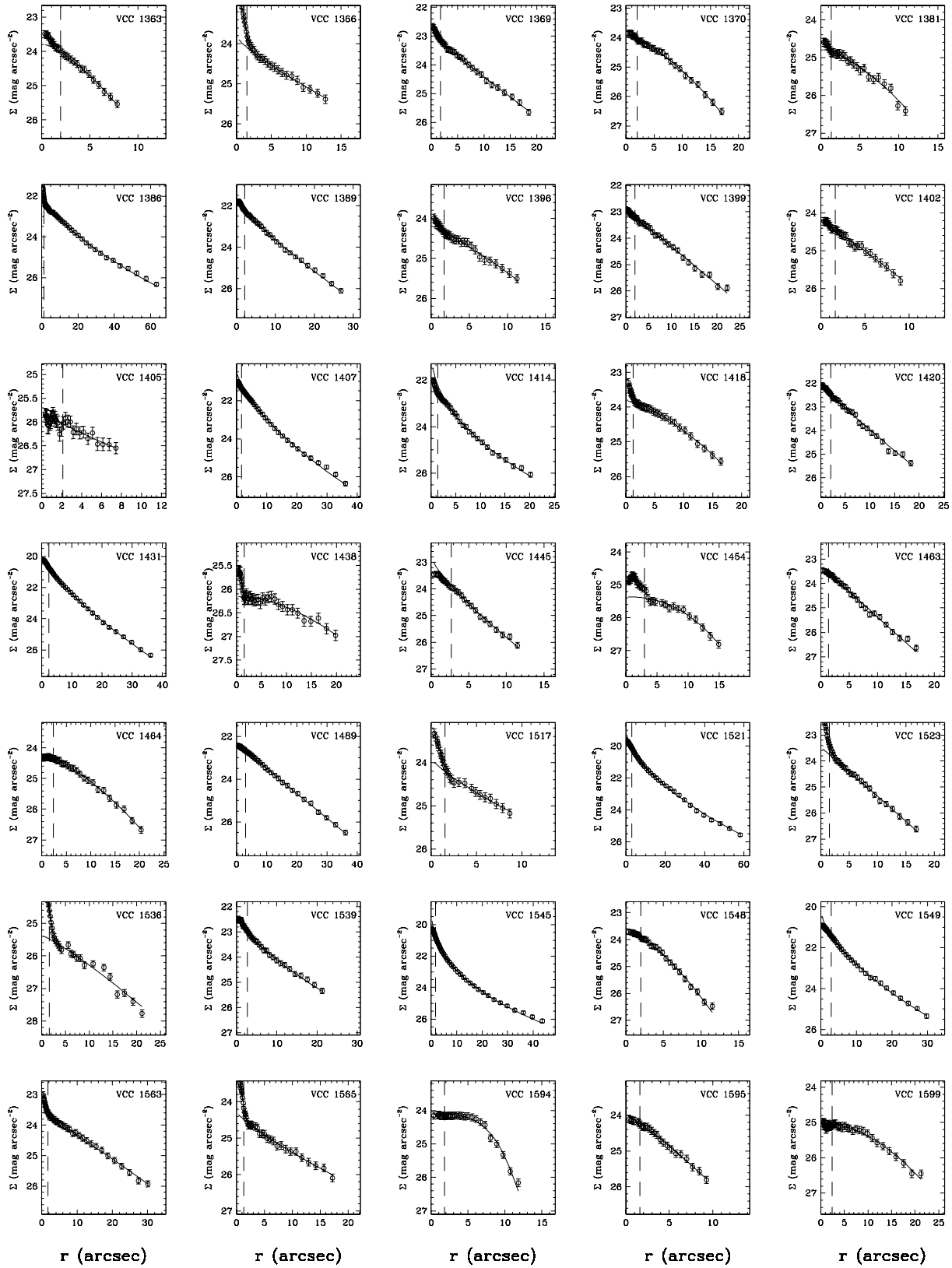

Fig. 13. continued.

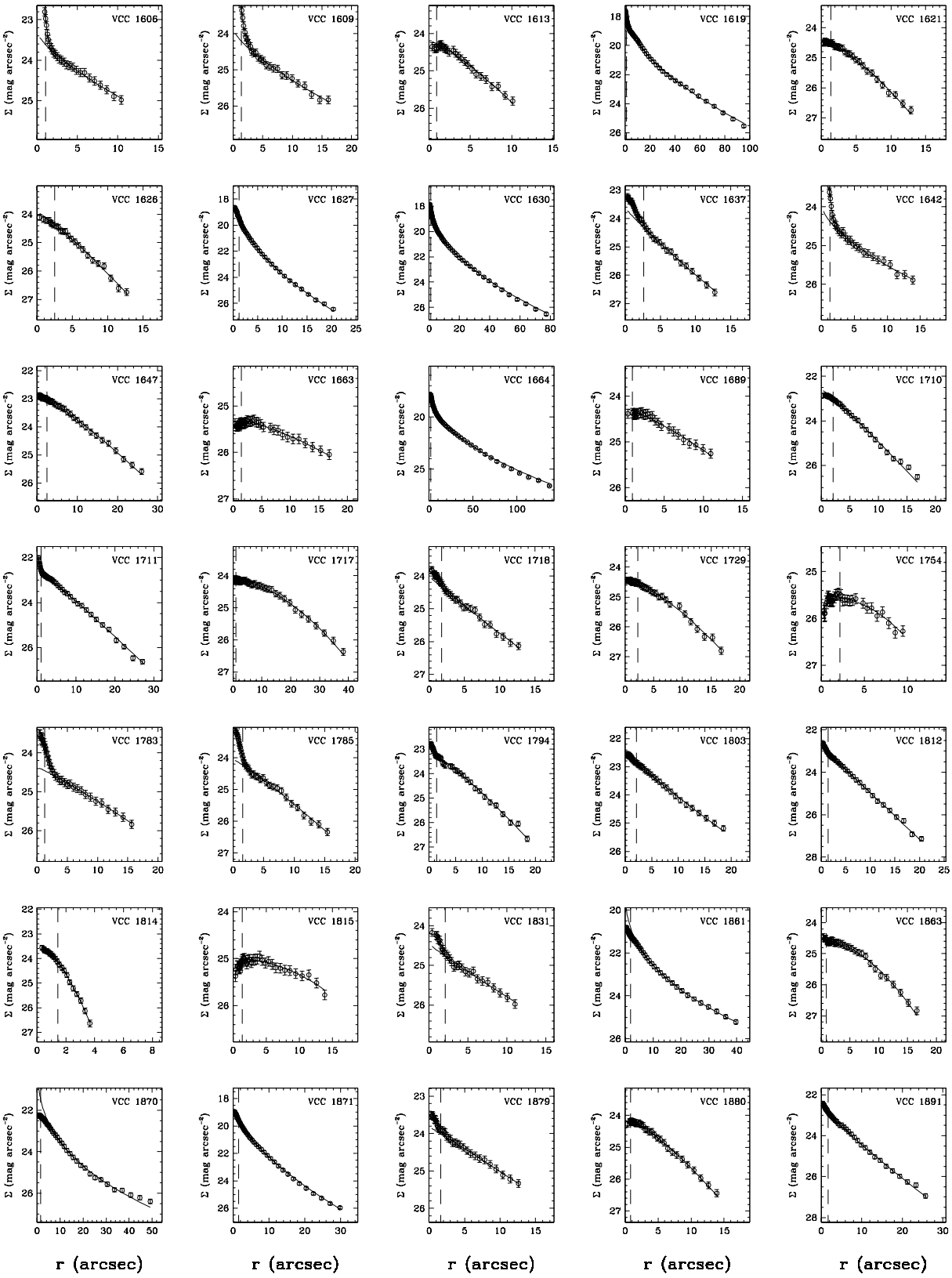

Fig. 13. continued.

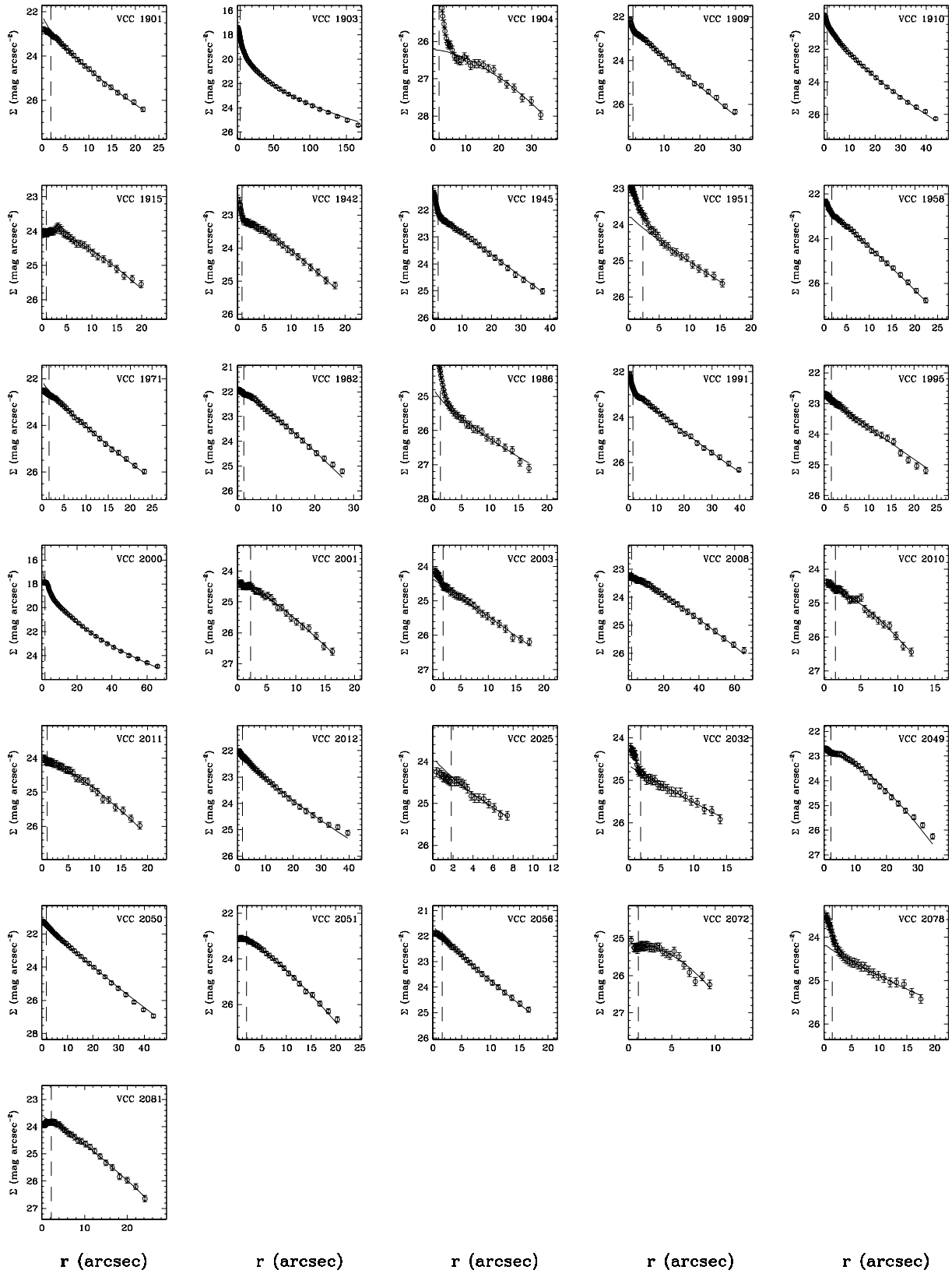

Fig. 13. continued.

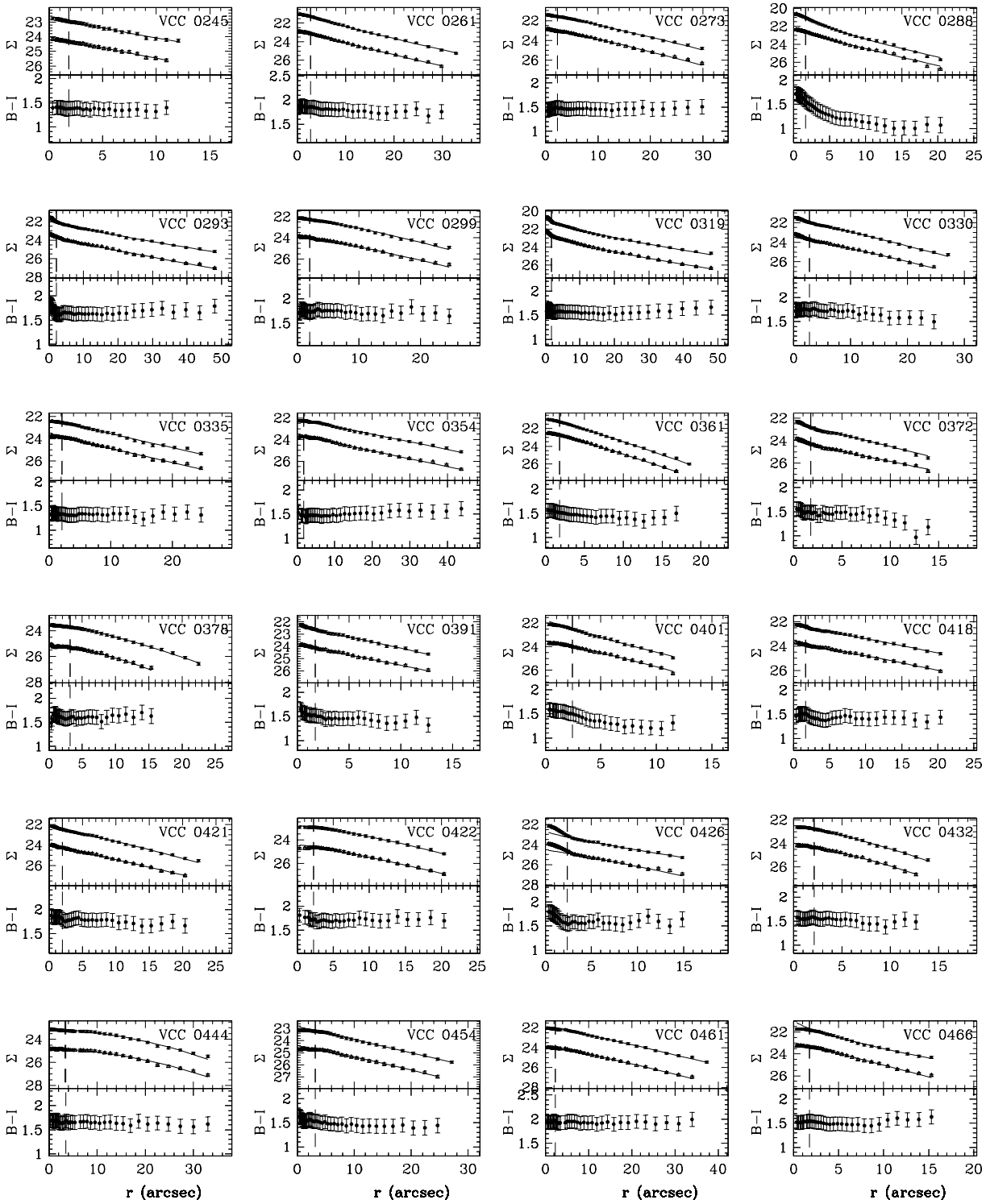

Fig. 14. The profiles and their Sersic fit for 90 galaxies in the WFV with *B* and *I* band imaging and their $B - I$ color profile. *I* Images are convolved to the seeing of *B* images, marked by the vertical dashed line.

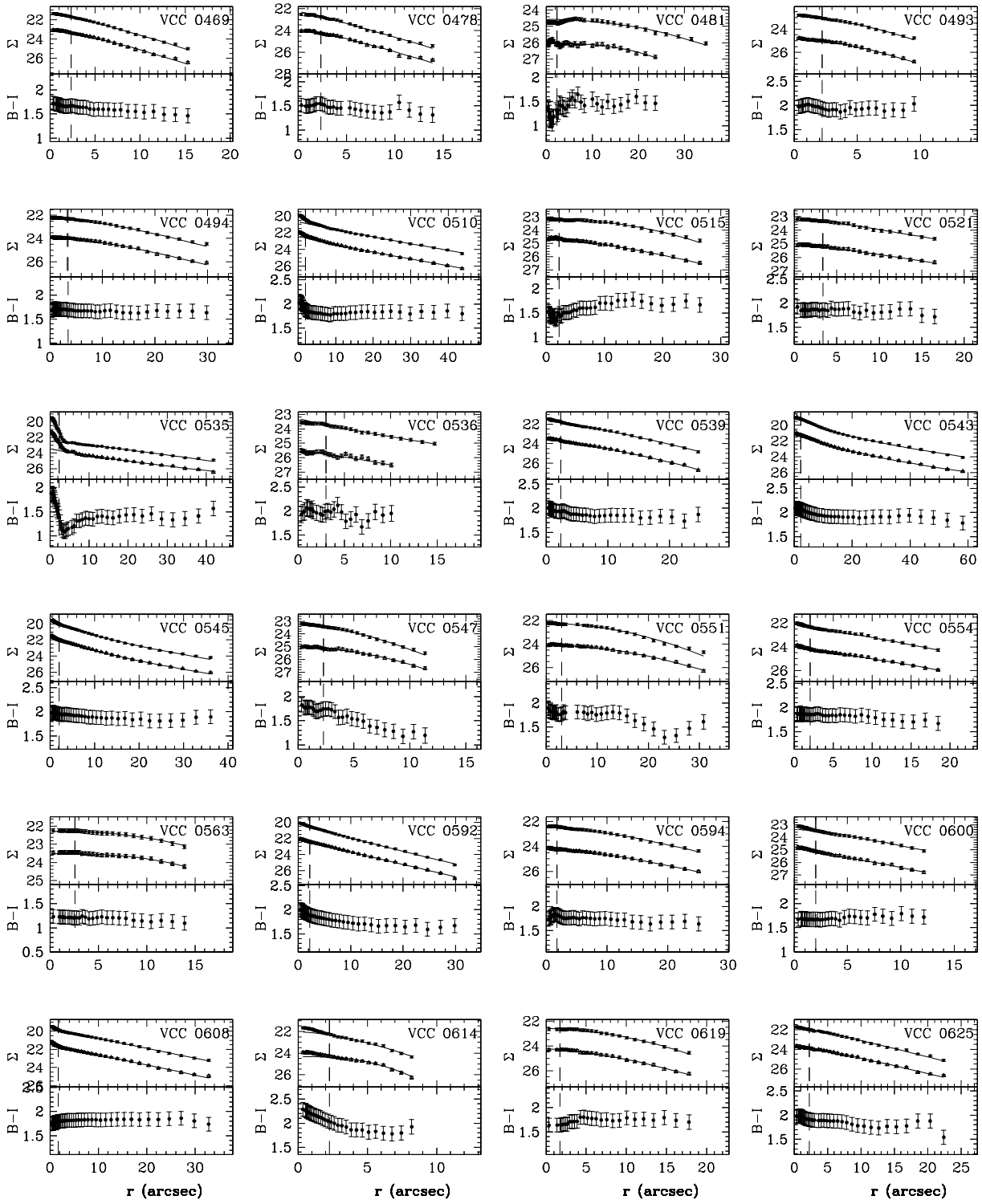

Fig. 14. continued.

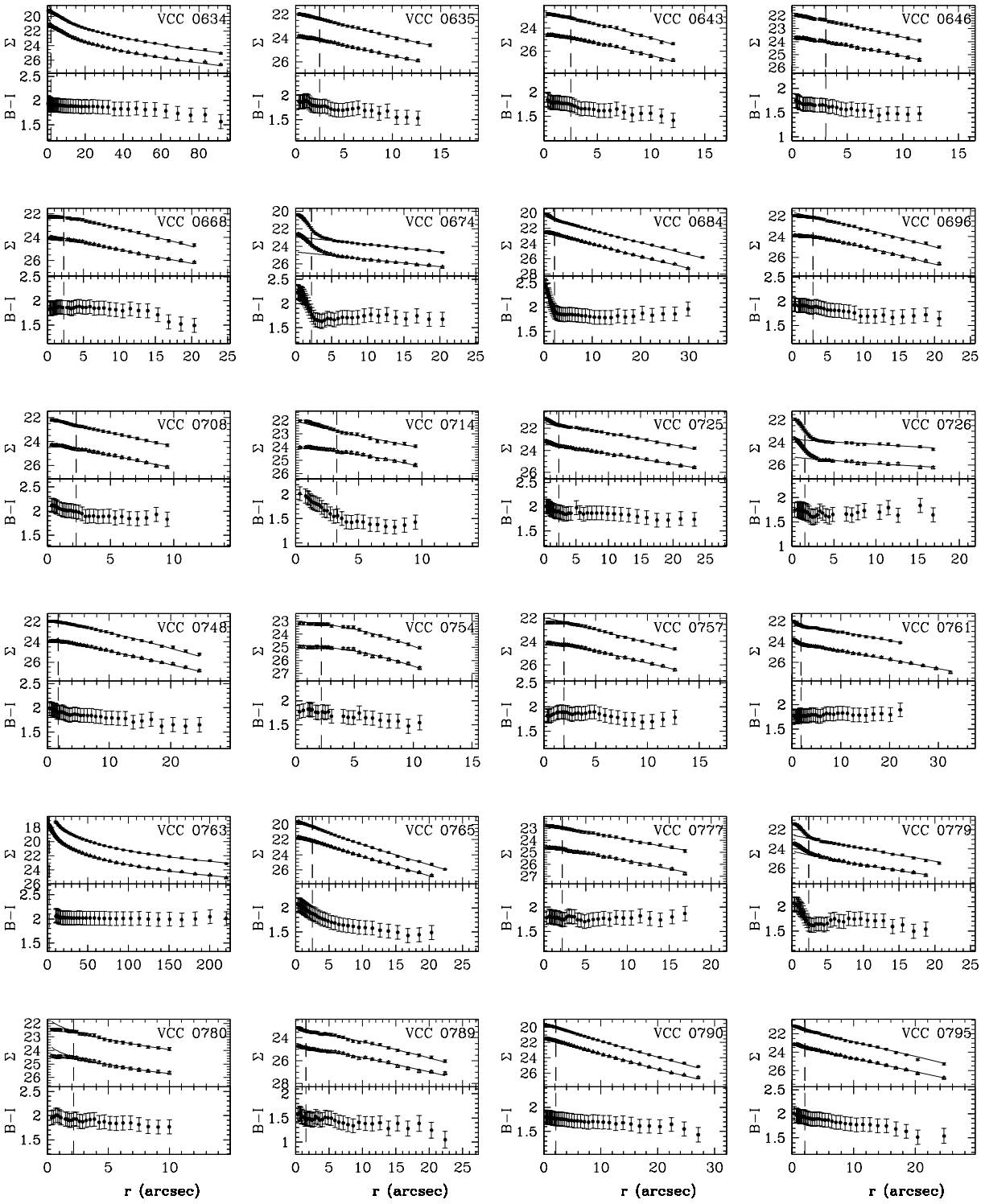

Fig. 14. continued.

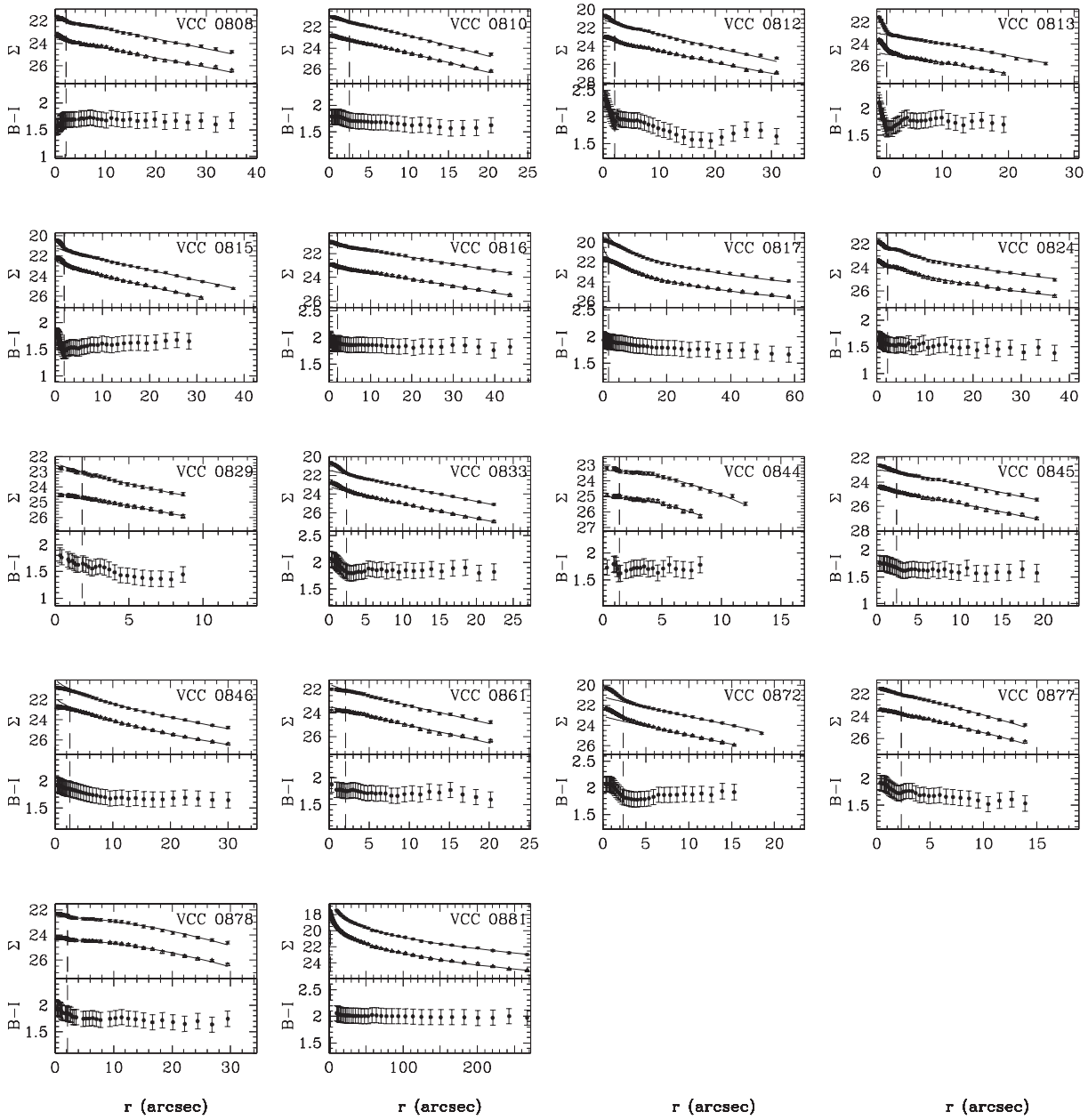

Fig. 14. continued.

Table 2: B-band parameters of the observed galaxies.

VCC (1)	Type (2)	(3)	m_p (4)	n (5)	μ_o (6)	B_T (7)	C_{31} (8)	$<\mu>_e$ (9)	r_e (10)	Strip (11)	Band (12)	Notes (13)	Ref (14)
245	dE	-	18.40	0.89	24.14	18.06	2.46	25.22	12.57	V	B,I		
261	dE	-	16.00	1.11	22.65	16.56	3.29	23.89	13.69	V	B,I		
273	dE	N	16.55	0.88	22.78	16.36	2.58	23.82	14.71	V	B,I		
288	dE	-	17.65	1.22	22.00	17.33	3.07	23.37	8.61	V	B,I	1	
293	dE	N	16.55	1.10	23.50	16.35	2.76	25.06	28.04	V	B,I		
299	dE	-	17.26	0.83	23.82	17.57	2.89	24.54	13.33	V	B,I		BJ98
319	dE	N	16.15	1.37	22.33	15.32	3.01	24.02	23.41	V	B,I		VPC
330	dE	N	16.65	0.89	23.45	16.98	2.75	24.46	13.95	V	B,I		VPC
335	dE	-	17.75	1.02	23.48	17.45	3.37	24.27	12.34	V	B,I		
354	dE	-	16.55	1.04	23.44	16.02	3.37	24.52	23.65	V	B,I		VPC,BJ98
361	dE	-	17.35	0.92	22.27	17.31	2.75	23.26	6.57	V	B,I		VPC
372	dE	N	17.95	1.04	23.95	18.20	2.76	25.31	10.82	V	B,I		
378	dE	-	18.75	0.62	25.11	18.60	2.43	25.64	10.42	V	B,I		
391	dE	-	17.97	0.95	23.83	17.88	2.85	24.96	10.81	V	B,I		
401	dE	-	17.65	0.79	23.62	18.14	2.67	24.49	7.79	V	B,I		
418	dE	-	17.84	0.88	23.75	17.41	2.84	24.76	15.53	V	B,I		
421	dE	-	16.95	0.94	23.99	17.82	2.64	25.20	12.76	V	B,I		
422	dE	-	17.95	0.83	24.37	17.88	2.76	25.42	14.02	V	B,I		
426	dE	N	18.12	0.88	24.51	18.53	2.47	25.49	10.15	V	B,I		
432	dE	-	18.95	0.75	24.05	19.04	3.39	24.95	7.53	V	B,I		
444	dE	-	17.17	0.55	24.77	17.61	2.10	25.46	19.94	V	B,I		BJ98
454	dE	-	17.55	0.89	24.43	17.88	3.12	25.40	16.11	V	B,I		
461	dE	-	16.45	0.87	23.79	16.92	2.68	24.89	18.74	V	B,I		VPC
466	dE	-	18.07	0.95	22.98	17.64	2.76	23.97	8.27	V	B,I		VPC
469	dE	-	18.50	0.80	23.00	17.99	2.67	23.82	7.25	V	B,I		
478	dE	-	18.58	0.80	23.90	18.94	2.54	24.53	6.77	V	B,I		
481	dE	-	18.30	0.34	26.05	18.54	1.71	26.45	19.20	V	B,I		
493	dE	-	18.95	0.63	24.73	19.73	2.34	25.30	6.23	V	B,I		
494	dE	-	16.59	0.68	23.82	16.68	2.33	24.59	19.03	V	B,I		VPC,BJ98
505	dE	N	17.75	0.72	25.17	17.61	2.37	26.07	24.79	V	B		
510	dE	N	15.07	1.11	22.33	15.20	3.14	23.98	23.90	V	B,I		BJ98
515	dE	-	18.15	0.70	24.58	17.14	2.44	25.24	19.81	V	B,I		
521	dE	-	18.45	0.97	24.83	18.22	3.21	26.00	19.56	V	B,I		
535	dE	-	16.95	1.22	23.38	16.28	3.82	24.31	23.81	V	B,I		
536	dE	-	18.95	0.31	25.72	19.83	1.91	25.83	7.58	V	B,I		
539	dE	N	16.75	0.73	23.60	17.01	2.62	24.22	12.80	V	B,I		VPC
543	dE	-	14.33	1.75	20.21	14.51	3.59	22.54	21.30	V	B,I		ACS,BJ98
545	dE	N	15.19	1.64	20.75	15.53	3.22	22.86	13.49	V	B,I	3	
547	dE	-	18.75	0.52	25.00	19.28	2.26	25.36	7.61	V	B,I		
551	dE	-	16.30	0.55	24.06	16.78	2.42	25.16	21.61	V	B,I		
554	dE	N	17.06	0.85	24.05	17.24	2.60	24.94	15.96	V	B,I		BJ98
563	dE	-	16.25	0.36	23.46	17.05	1.86	23.78	11.83	V	B,I		
592	dE	N	16.55	1.05	21.95	16.55	3.29	22.94	10.64	V	B,I		VPC
594	dE	-	17.08	0.68	24.14	17.40	2.50	24.81	18.41	V	B,I		BJ98
600	dE	-	17.95	0.91	24.86	19.05	2.41	25.89	11.12	V	B,I		
608	dE	N	14.86	0.94	21.53	14.94	2.64	22.92	18.27	V	B,I		BJ98
614	dE	-	18.55	0.39	24.28	19.17	2.30	24.47	4.84	V	B,I		
619	dE	-	18.15	0.65	24.17	18.09	2.26	24.81	11.79	V	B,I		
625	dE	-	18.15	0.88	23.59	17.76	2.85	24.70	12.47	V	B,I		
634	dE	N	14.08	2.78	18.87	13.99	4.09	22.92	27.61	V	B,I		
635	dE	-	18.95	1.09	23.56	18.44	3.62	25.40	12.40	V	B,I		
643	dE	-	18.45	0.76	24.50	19.05	2.87	25.25	7.57	V	B,I		
646	dE	-	18.75	0.76	23.70	17.70	2.65	24.53	10.07	V	B,I		
663	dE	-	18.15	0.86	23.67	17.28	2.91	24.48	14.53	V	B		
668	dE	-	16.45	1.08	23.70	17.42	3.39	24.95	14.49	V	B,I		VPC
674	dE	N	17.95	1.00	24.59	17.14	3.15	25.79	22.20	V	B,I		
677	dE	-	18.15	0.65	23.74	17.85	2.32	24.46	8.56	V	B		
684	dE	N	15.98	1.11	22.15	16.32	2.79	23.55	11.37	V	B,I		VPC,BJ98
696	dE	-	18.25	0.84	23.64	17.75	2.55	24.41	10.83	V	B,I		
708	dE	N	18.95	1.00	24.05	18.81	2.51	25.04	7.48	V	B,I		
714	dE	-	18.25	0.68	24.00	18.28	2.44	24.70	9.03	V	B,I		
725	dE	N	15.95	0.94	23.39	16.20	2.35	24.74	21.08	V	B,I		
726	dE	N	18.65	1.16	25.24	19.16	2.09	25.87	12.14	V	B,I		
748	dE	-	17.25	0.89	23.68	17.53	3.04	24.73	13.20	V	B,I		VPC
754	dE	-	18.95	0.54	24.80	19.34	1.95	25.35	7.49	V	B,I		
757	dE	-	18.55	0.93	23.82	18.58	2.89	24.91	8.53	V	B,I		
761	dE	-	17.21	0.95	24.06	17.22	3.06	25.11	21.51	V	B,I		BJ98
763 M84	E	-	10.20	7.14	8.74	10.22	5.29	20.61	48.55	V	B,I	3,6,4	ACS*
765	dE	N	16.43	1.12	21.19	16.49	2.79	22.54	6.72	V	B,I		VPC,BJ98
777	dE	-	17.95	0.88	24.50	17.91	2.65	25.53	14.17	V	B,I		
779	dE	N	17.62	1.25	24.10	17.74	3.56	25.54	15.42	V	B,I		BJ98
780	dE	-	18.27	2.50	22.99	18.89	5.75	25.11	7.53	V	B,I		
789	dE	-	18.95	0.81	24.76	18.54	2.92	25.71	14.69	V	B,I		
790	dE	N	16.34	1.14	21.07	15.90	2.88	22.70	9.53	V	B,I		VPC
795	dE	N	17.95	1.05	23.08	17.60	3.19	24.09	11.17	V	B,I		VPC
797	dE	N	16.94	1.33	21.59	16.49	3.26	22.92	9.32	V	B		
808	dE	N	17.65	0.99	23.54	16.74	3.10	24.46	19.25	V	B,I		VPC
810	dE	N	16.91	0.91	22.86	16.86	2.68	23.71	9.67	V	B,I		B03,VPC,BJ98
812	dE	N	16.98	1.10	23.00	16.88	2.89	24.16	13.15	V	B,I		VPC
813	dE	N	18.15	0.93	24.78	17.59	2.84	25.75	18.01	V	B,I		
815	dE	N	16.06	1.45	22.13	16.16	3.12	23.87	15.61	V	B,I		B03.VPC,BJ98

Table 2: Continued

VCC (1)	Type (2)	(3)	m_p (4)	n (5)	μ_o (6)	B_T (7)	C_{31} (8)	$<\mu>_e$ (9)	r_e (10)	Strip (11)	Band (12)	Notes (13)	Ref (14)
816	dE	N	15.25	0.97	23.01	15.18	2.53	24.29	33.51	V	B,I		
817	dE	-	14.93	3.70	18.92	14.66	3.35	23.05	21.35	V	B,I		
824	dE	N	17.95	2.08	22.77	16.56	3.09	25.13	23.64	V	B,I		
829	dE	-	18.45	0.90	24.39	19.01	2.89	25.34	9.59	V	B,I		
833	dE	N	17.42	1.15	23.12	17.24	3.04	24.34	10.97	V	B,I		VPC
844	dE	-	18.85	0.52	24.98	19.77	2.20	25.50	6.61	V	B,I		
845	dE	-	18.95	0.92	24.52	18.77	2.89	25.28	11.71	V	B,I		
846	dE	N	16.16	1.61	21.64	16.39	3.11	23.61	12.50	V	B,I		B03,VPC
861	dE	-	17.85	1.06	23.38	17.72	3.15	24.34	10.90	V	B,I		
872	dE	N	16.93	1.04	23.04	17.23	3.25	23.92	9.21	V	B,I		BJ98
877	dE	N	17.55	0.83	23.39	17.90	2.58	24.22	7.56	V	B,I		
878	dE	-	17.25	0.57	24.30	17.15	2.13	24.83	18.44	V	B,I		
881 M86	E	-	10.01	3.45	16.31	10.19	5.15	20.89	64.16	V	B,I	3,4	ACS*
882	dE	N	16.63	1.19	21.57	15.76	2.99	22.99	12.88	V	B		
1083	dE	-	19.00	0.49	24.75	19.89	2.13	25.15	5.38	H	B		
1104	dE	N	15.14	1.08	21.45	15.42	3.12	22.61	13.30	H	B	3	B03,VPC,BJ98
1111	dE	N	17.65	0.84	23.34	17.62	2.45	24.34	9.85	H	B		
1123	dE	N	16.60	1.09	23.51	16.79	2.83	24.95	18.22	H	B		VPC
1129	dE	-	17.64	0.81	23.36	17.82	2.50	24.28	8.36	H	B		B03
1131	dE	-	18.05	0.87	24.67	18.01	3.07	25.45	14.89	H	B		
1136	dE	N	17.97	0.49	25.25	18.53	2.09	25.84	14.65	H	B		
1148	E	-	15.90	2.22	18.32	16.21	3.60	21.21	4.11	H	B		VPC
1153	dE	-	17.75	0.57	23.64	17.97	2.19	24.29	9.22	H	B		
1161	dE	-	18.98	0.65	24.83	19.18	2.32	25.45	8.62	H	B		
1177	dE	-	18.65	0.85	24.44	18.67	2.77	25.60	10.87	H	B		
1185	dE	N	15.62	1.52	21.72	15.57	3.17	23.55	16.76	H	B		VPC,ACS,BJ98
1191	dE	N	17.37	0.87	23.68	17.61	2.86	24.34	11.25	H	B		
1213	dE	N	16.37	1.32	22.80	16.37	3.06	24.24	15.61	H	B		VPC,BJ98
1219	dE	N	18.16	0.84	23.34	18.37	2.88	24.32	6.71	H	B		
1239	dE	N	17.75	1.14	22.85	17.26	19.21	24.65	19.00	H	B		
1259	dE	-	18.19	0.51	24.43	18.21	2.16	24.96	12.36	H	B		
1264	dE	N	17.26	1.16	23.42	16.60	2.96	24.79	17.60	H	B		BJ98
1279	E	-	12.08	2.56	14.96	12.20	4.13	19.70	13.68	H	B	3,5	F97,ACS
1286	dE	-	18.80	1.49	24.75	18.93	4.33	27.08	19.05	H	B		
1291	dE	-	18.77	0.86	24.97	18.50	2.63	25.88	14.60	H	B		
1297	E	-	14.26	2.38	14.26	14.20	3.63	18.45	3.01	H	B	1,2,4	F97,ACS
1308	dE	N	15.56	2.38	18.98	15.64	3.49	22.01	10.69	H	B	3	VPC,BJ98
1312	dE	-	18.65	0.59	25.01	19.14	2.37	25.60	11.29	H	B		
1316 M87	E	-	9.51	3.85	15.07	9.80	4.95	20.48	63.53	H	B	4	F97.ACS
1317	dE	N	17.93	1.28	22.76	18.13	3.12	24.03	6.79	H	B		
1327	E	-	13.20	5.00	8.10	13.11	5.12	19.12	7.01	H	B	1,2,4	ACS*
1348	dE	-	15.79	2.17	19.82	15.87	3.34	22.40	8.80	H	B		VPC,BJ98
1352	dE	-	17.15	1.27	22.70	17.19	3.14	24.02	11.51	H	B		VPC
1353	dE	N	16.56	1.05	21.71	16.54	3.08	22.87	8.20	H	B		VPC,BJ98
1363	dE	N	18.93	0.69	23.73	18.86	2.72	24.31	5.86	H	B		
1366	dE	N	17.55	1.23	23.77	16.98	3.41	25.25	19.19	H	B		
1369	dE	N	17.23	1.10	22.76	17.03	3.00	24.03	13.07	H	B		VPC
1370	dE	-	17.35	0.65	23.95	17.66	2.14	24.57	9.89	H	B		
1381	dE	-	18.95	0.65	24.74	18.90	2.27	25.37	9.12	H	B		
1386	dE	N	14.25	1.59	21.53	14.88	3.54	23.52	27.11	H	B		VPC
1389	dE	N	15.85	1.19	21.65	16.09	3.25	22.92	11.09	H	B		VPC,BJ98
1396	dE	N	17.16	0.83	24.17	17.57	2.57	25.15	13.17	H	B		BJ98
1399	dE	N	16.44	0.96	22.92	17.19	3.13	23.76	11.73	H	B		BJ98
1402	dE	N	17.95	0.89	24.19	18.36	2.65	25.18	9.95	H	B		
1405	dE	-	18.95	1.27	25.70	20.76	1.92	26.15	5.34	H	B		
1407	dE	N	15.43	1.54	20.29	15.18	3.39	22.37	11.81	H	B	3	VPC,ACS,BJ98
1414	dE	-	16.95	2.17	20.60	17.42	3.35	23.15	7.53	H	B	3	
1418	dE	-	17.37	0.68	23.77	17.49	2.37	24.57	13.03	H	B		
1420	dE	N	16.34	1.09	21.96	16.53	3.13	23.00	9.48	H	B		VPC,BJ98
1431	dE	N	14.43	1.37	19.76	14.53	3.17	21.54	10.10	H	B		ACS
1438	dE	-	17.82	0.54	26.10	18.05	2.22	26.56	20.60	H	B		
1445	dE	-	18.37	1.28	22.76	18.33	2.88	24.17	6.56	H	B		
1454	dE	N	18.64	0.43	25.32	18.57	2.10	25.69	10.88	H	B		
1463	dE	-	18.45	1.01	23.22	18.51	2.93	23.88	7.29	H	B		
1464	dE	-	17.67	0.70	24.18	17.81	2.53	24.88	12.84	H	B		
1489	dE	-	15.84	1.03	22.22	16.04	3.07	23.24	14.72	H	B		VPC,ACS
1517	dE	N	17.25	1.30	23.84	18.01	2.41	24.86	10.46	H	B		
1521	E	-	14.14	1.72	18.87	14.09	4.19	20.74	14.51	H	B		
1523	dE	N	17.59	0.97	23.43	17.68	2.94	24.35	8.98	H	B		BJ98
1536	dE	N	18.35	0.85	25.32	18.69	3.38	26.20	15.28	H	B		
1539	dE	N	15.61	1.37	22.31	16.09	3.03	23.94	15.67	H	B		VPC,ACS,BJ98
1545	E	-	14.88	2.63	18.48	15.08	4.27	21.90	11.34	H	B		ACS
1548	dE	-	18.54	0.68	23.63	19.02	2.34	24.17	5.75	H	B		
1549	dE	N	14.56	1.67	20.03	15.07	3.41	21.93	10.51	H	B		VPC
1563	dE	N	16.06	0.97	23.50	16.27	2.90	24.54	22.19	H	B		VPC,BJ98
1565	dE	N	16.86	1.23	24.22	17.11	3.36	25.74	22.57	H	B		VPC
1594	dE	-	18.68	0.28	24.06	18.91	1.54	24.59	7.78	H	B		
1595	dE	-	18.33	0.85	23.96	18.49	2.68	24.87	8.32	H	B		
1599	dE	-	17.25	0.52	24.96	17.95	1.96	25.49	15.50	H	B		
1606	dE	N	17.45	1.39	23.25	17.17	4.22	24.99	16.81	H	B		
1609	dE	N	17.32	1.37	23.83	17.14	3.92	25.34	18.09	H	B		
1613	dE	-	18.45	0.78	24.15	18.67	2.63	24.98	9.07	H	B		

Table 2: Continued

VCC (1)	Type (2)	(3)	m_p (4)	n (5)	μ_o (6)	B_T (7)	C_{31} (8)	$<\mu>_e$ (9)	r_e (10)	Strip (11)	Band (12)	Notes (13)	Ref (14)
1619	E	-	12.44	1.79	17.51	12.42	3.91	19.59	19.36	H	B	4	ACS*
1621	dE	-	18.32	0.73	24.34	19.02	2.66	24.94	7.58	H	B		
1626	dE	-	18.95	0.85	23.88	18.84	2.60	24.79	7.48	H	B		
1627	E	-	15.11	1.92	17.31	15.37	3.82	20.24	3.83	H	B		ACS
1630	E	-	12.84	1.92	17.72	12.82	4.23	20.48	15.21	H	B	5	F97,ACS
1637	dE	N	18.45	1.11	23.56	18.26	3.03	24.76	8.11	H	B		
1642	dE	N	17.75	1.64	23.86	17.48	5.13	25.81	19.36	H	B		
1647	dE	-	15.95	0.85	22.77	16.23	2.66	23.72	15.51	H	B		VPC
1663	dE	-	17.45	0.71	25.22	17.33	2.35	25.86	23.32	H	B		
1664	E	-	11.95	1.92	17.54	11.90	6.10	20.30	24.75	H	B	5	F97,ACS
1689	dE	-	16.95	0.79	24.23	17.46	2.51	25.07	14.62	H	B		
1710	dE	-	17.75	0.90	22.54	17.57	2.68	23.41	6.97	H	B		
1711	dE	N	16.43	0.93	22.47	16.38	2.81	23.55	11.95	H	B		VPC,BJ98
1717	dE	-	16.45	0.57	24.08	16.91	2.15	24.60	22.97	H	B		BJ98
1718	dE	N	18.25	1.05	23.96	18.48	2.86	25.13	10.67	H	B		
1729	dE	-	17.75	0.68	24.39	18.63	2.73	24.92	10.19	H	B		
1754	dE	-	18.95	0.45	25.47	19.42	1.98	25.87	8.73	H	B		
1783	dE	N	18.17	0.91	24.32	17.78	2.80	25.28	17.75	H	B		
1785	dE	N	17.75	0.89	24.00	17.93	2.59	24.93	11.11	H	B		
1794	dE	N	17.25	0.83	23.08	17.94	2.74	23.77	8.48	H	B		
1803	dE	N	16.65	1.14	22.36	16.23	2.94	23.73	12.86	H	B		
1812	dE	N	17.73	0.98	22.77	17.63	3.02	23.69	7.90	H	B		BJ98
1814	dE	-	18.65	0.65	23.33	20.88	2.30	23.91	1.82	H	B		
1815	dE	-	17.31	0.49	24.95	17.92	1.92	25.08	13.73	H	B		
1831	dE	N	17.95	1.08	24.41	17.94	3.10	25.72	15.25	H	B		
1861	dE	N	14.31	2.56	18.83	14.46	3.14	22.29	15.04	H	B	3	ACS
1863	dE	-	18.94	0.54	24.51	18.75	2.15	24.87	9.07	H	B		
1870	dE	-	15.73	2.94	19.07	16.22	3.39	22.92	14.62	H	B	3	
1871	E	-	13.80	1.61	18.31	14.43	3.41	20.67	7.17	H	B		ACS
1879	dE	N	17.25	0.95	23.78	17.32	2.79	24.90	14.64	H	B		
1880	dE	-	18.48	0.75	24.04	18.51	2.66	24.77	8.79	H	B		
1891	dE	N	16.63	1.16	22.37	17.16	3.31	23.72	10.41	H	B		
1901	dE	-	17.55	1.41	22.03	17.44	3.15	23.59	9.56	H	B		
1903	E	-	10.70	3.03	15.80	10.88	5.53	20.60	39.47	H	B	1,5	F97,ACS
1904	dE	N	18.95	0.60	26.17	17.72	2.66	26.50	22.86	H	B		
1909	dE	N	16.05	1.04	22.35	16.50	3.22	23.39	12.78	H	B		
1910	dE	N	14.12	1.47	19.79	14.41	3.13	21.86	13.22	H	B		ACS
1915	dE	-	17.08	0.68	23.89	17.20	2.65	24.42	14.58	H	B		BJ98
1942	dE	N	16.72	0.79	23.03	16.81	2.85	23.96	13.33	H	B		BJ98
1945	dE	N	14.77	1.01	22.00	15.23	3.48	23.15	21.61	H	B		
1951	dE	N	16.95	1.16	23.66	16.92	3.14	24.91	16.10	H	B		
1958	dE	N	16.93	0.92	22.57	16.88	2.86	23.52	9.45	H	B		
1971	dE	-	16.53	1.19	22.02	16.72	3.24	23.35	10.78	H	B		
1982	dE	-	15.24	0.87	21.84	16.02	2.72	22.84	13.67	H	B	1	
1986	dE	N	18.95	1.35	24.68	18.16	3.55	26.11	16.00	H	B		
1991	dE	N	15.55	1.12	22.54	15.66	2.91	23.93	20.13	H	B		
1995	dE	-	15.75	1.05	22.64	15.90	2.81	23.95	18.18	H	B		
2000	E	-	11.87	2.17	16.03	12.11	4.84	19.46	13.56	H	B	3,5	ACS*
2001	dE	-	18.95	0.79	24.26	18.02	2.54	25.16	11.46	H	B		
2003	dE	-	18.15	0.96	24.33	17.98	3.06	25.34	15.50	H	B		
2008	dE	-	14.95	0.86	23.16	15.06	2.72	24.21	40.74	H	B		
2010	dE	-	18.95	0.69	24.42	18.88	2.39	25.07	8.35	H	B		
2011	dE	-	17.05	0.72	24.00	17.40	2.61	24.65	13.05	H	B		
2012	dE	N	14.22	1.30	21.77	14.74	2.97	23.30	22.42	H	B	1	
2025	dE	-	18.45	1.32	23.80	18.34	3.83	25.62	13.80	H	B		
2032	dE	-	17.45	1.08	24.60	17.18	2.95	25.91	24.12	H	B		
2049	dE	N	16.35	0.65	22.72	16.52	2.38	23.26	15.19	H	B	1	
2050	dE	N	15.13	1.12	21.05	15.23	3.03	22.98	16.37	H	B		ACS
2051	dE	-	17.45	0.78	22.91	17.24	2.65	23.75	9.29	H	B		
2056	dE	-	16.95	1.15	21.53	16.43	3.18	22.98	9.59	H	B		
2072	dE	-	18.95	0.47	25.10	19.54	1.76	25.53	7.31	H	B		
2078	dE	-	17.45	1.15	24.10	16.26	3.24	25.49	32.61	H	B		
2081	dE	-	16.95	0.82	23.59	17.11	2.70	24.47	13.82	H	B		

Column 1: VCC designation.
Column 2,3: Morphological type from the VCC. N=Nucleated.
Column 4: Photographic magnitude m_p from the VCC.
Column 5: Sersic index n.
Column 6: Sersic extrapolation to $r = 0$ of the central surface brightness μ_o (in mag arcsec^{-2}).
Column 7: Total asymptotic magnitude B_T.
Column 8: Light concentration index C_{31}.
Column 9: Mean effective surface brightness $<\mu>_e$ (in mag arcsec^{-2}).
Column 10: Effective major-axis radius r_e (in arcsec).
Column 11: WFS strip: H=horizontal; V=vertical.
Column 12: Available band(s).
Column 13: Notes. (1 = poor outer fit; 2 = M32 like object; 3 = two seeing disks excluded from the fit; 4 = core; 5 = power law; 6 = saturated.
Column 14: Reference to other works. B03 = Barazza et al (2003), F97 = Faber et al. (1997), VPC = Young & Currie (1998), BJ98 = Binggeli & Jerijn 1998; ACS = in The ACS Virgo Cluster Survey, ASC*= whether core or power law, kindly provided by Laura Ferrarese (private communication).